Journal of Computer-Aided Molecular Design, **13:** 325–353, 1999.
KLUWER/ESCOM

Perspective

Structural organization of G-protein-coupled receptors

Andrei L. Lomize, Irina D. Pogozheva & Henry I. Mosberg*
College of Pharmacy, University of Michigan, Ann Arbor, MI 48109-1065, U.S.A.

Received 15 July 1998; Accepted 17 November 1998

Key words: distance geometry, H-bonding, membrane proteins, molecular modeling, protein structure

Summary

Atomic-resolution structures of the transmembrane 7-α-helical domains of 26 G-protein-coupled receptors (GPCRs) (including opsins, cationic amine, melatonin, purine, chemokine, opioid, and glycoprotein hormone receptors and two related proteins, retinochrome and Duffy erythrocyte antigen) were calculated by distance geometry using interhelical hydrogen bonds formed by various proteins from the family and collectively applied as distance constraints, as described previously [Pogozheva et al., Biophys. J., 70 (1997) 1963]. The main structural features of the calculated GPCR models are described and illustrated by examples. Some of the features reflect physical interactions that are responsible for the structural stability of the transmembrane α-bundle: the formation of extensive networks of interhelical H-bonds and sulfur–aromatic clusters that are spatially organized as 'polarity gradients'; the close packing of side-chains throughout the transmembrane domain; and the formation of interhelical disulfide bonds in some receptors and a plausible Zn^{2+} binding center in retinochrome. Other features of the models are related to biological function and evolution of GPCRs: the formation of a common 'minicore' of 43 evolutionarily conserved residues; a multitude of correlated replacements throughout the transmembrane domain; an Na^{+}-binding site in some receptors, and excellent complementarity of receptor binding pockets to many structurally dissimilar, conformationally constrained ligands, such as retinal, cyclic opioid peptides, and cationic amine ligands. The calculated models are in good agreement with numerous experimental data.

Introduction

The rhodopsin-like G-protein-coupled receptors (GPCRs) form a unique family of hundreds of proteins which transduce chemical and optical signals through the cytoplasmic membrane by activating intracellular G-proteins [1]. Electron microscopy studies of several rhodopsins [2–4] have clearly shown that these receptors consist of seven transmembrane α-helices. Furthermore, the presence, in each transmembrane helix, of several characteristic residues conserved throughout the rhodopsin-like GPCRs indicates that all proteins in the family share a common 3D structure [5]. The existence of a minimum sequence homology of ∼20% between remotely related GPCRs leads to an estimated 1.6–2.3 Å root mean square deviation (rmsd) of main-chain atoms within the α-helical core, using a calibration curve relating the coordinate rmsd and sequence identity for proteins with known 3D structures [6].

GPCRs, especially rhodopsin itself, have been extensively studied by site-directed mutagenesis and by a variety of physicochemical methods. These experimental data and the analysis of variability and hydrophobicity patterns in amino acid sequences of GPCRs have made possible the identification of the transmembrane helices of GPCRs and their unequivocal assignment to the peaks in EM maps [5] and the construction of various approximate GPCR models. Modeling of the transmembrane domain is simplified by the identification of residues that are evolutionarily conserved or hydrophilic, or which are important for folding or ligand binding of GPCRs. These residues form the protein interior, thus defining a lipid-inaccessible surface of each transmembrane helix and

*To whom correspondence should be addressed.

Table 1. GPCR transmembrane α-bundle models calculated by distance geometry with H-bonding constraints; the listed agonists and antagonists were docked with the receptor models

	Identifier	Accession number	Receptor name	Agonists	Antagonists
1	OPRD_BOVIN	P02699	Bovine rhodopsin	All-*trans* retinal	11-*cis* retinal
2	OPSR_HUMAN	P04000	Red cone opsin	All-*trans* retinal	11-*cis* retinal
3	OPSB_HUMAN	P03999	Blue cone opsin	All-*trans* retinal	11-*cis* retinal
4	OPSD_XENLA	P29403	Frog rhodopsin	All-*trans* retinal	11-*cis* retinal
5	OPSD_PROCL	P35356	Crayfish Rhodopsin	All-*trans* retinal	11-*cis* retinal
6	REIS_TODPA	P23820	Squid Retinochrome	11-*cis* retinal	All-*trans* retinal
7	A2AA_HUMAN	P08913	α_{2A}-adrenergic	Clonidine	
8	B2AR_HUMAN	P07550	β_2-adrenergic Isopreterenol	Epinephrine	Carazolol, iodoazidobenzylpindolol
9	D2DR_HUMAN	P14416	Dopamine D_{2A}	Dopamine	Spiperone
10	5H1A_HUMAN	P08908	Serotonin $5HT_{1A}$	Serotonin	Spiperone
11	HH2R_HUMAN	P25021	Histamine H_2	Histamine	
12	ACM1_HUMAN	P11229	Muscarinic m_1	Acetylcholine	Atropine, pirenzepine
13	ACM3_HUMAN	P20309	Muscarinic m_3	Acetylcholine	
14	ML1A_HUMAN	P48039	Melatonin	Melatonin	
15	OPRD_HUMAN	P41143	δ-opioid	JOM-13	Naltrindole
16	OPRM-MOUSE	P42866	μ-opioid	Morphine	Naloxone
17	OPRK_HUMAN	P41145	κ-opioid	U69,593	Norbinaltorphimine
18	OPRX_HUMAN	P41146	Orphanin		
19	IL8A_HUMAN	P25024	CXC chemokine		
20	IL8B_HUMAN	P25025	CXC chemokine		
21	LCR1_HUMAN	P30991	CXC fusin		
22	CKR5_HUMAN	P51681	CC chemokine		
23	US28_HCMVA	P09704	CC chemokine		
24	G74_HSUSA	Q01035	*Herpesvirus saimiri*		
25	HSDARC	X85785	Duffy antigen		
26	AA2A_HUMAN	P29274	Adenosine A2A	Adenosine	
27	P2UR_HUMAN	P41231	ATP	ATP	
28	LSHR_HUMAN	P22888	Lutropin/choriogonadotropin		

Coordinates for all receptor models listed are available from our Web site at http://www.umich.edu/∼him. The structures of bovine rhodopsin complexed with 11-*cis* retinal and all-*trans* retinal have been deposited in the Protein Data Bank (PDB files: 1bok and 1boj, respectively).

placing a restriction on rotational orientation of the helix and the depth of its immersion into the α-bundle [5,7,8]. GPCR models typically have been built from seven 'ideal' helices with arbitrarily chosen side-chain conformers (or without side chains at all) to satisfy the published two-dimensional EM maps, restrictions on rotational orientations of the helices, and some constraints derived from mutagenesis and cross-linking data [9–14]. Perhaps the best model of this type has recently been developed by fitting two kinked and five straight α-helices to electron cryomicroscopy three-dimensional (3D) maps of frog rhodopsin [15]. Nevertheless, the resolution currently achieved by electron microscopy of rhodopsins (∼7.5 Å in the membrane plane and 16.5 Å in the perpendicular direction, Reference 3) is insufficient to obtain atomic-level structure, since individual residues are not visible in the maps. Therefore, we have developed, specifically for the modeling of GPCRs, a purely geometrical approach that relies on distance constraints, as in calculations of protein structures from NMR spectroscopy data [16]. The approach consists of an iterative distance geometry refinement of an approximate initial model using an evolving system of hydrogen bonds, formed by intramembrane polar side-chains in various proteins in the family and collectively applied as distance

constraints [16,17]. The models of 26 rhodopsin-like GPCRs and two related proteins have been calculated using this method (Table 1).

Three features make GPCRs especially attractive for structural analysis: (i) Similar to bacteriorhodopsin, apoferritin, and glucoamylase, GPCRs form α-bundles containing many polar residues within a generally hydrophobic protein 'core'. This accentuates the clustering of residues with similar polarities, which is less apparent in structures of typical water-soluble proteins with more uniformly nonpolar interiors. (ii) The sequence identity between remotely related members of the family is only ∼20% within the common transmembrane core. This provides an opportunity to compare many different variations of side-chain packing, all of which must be compatible within essentially the same 3D structure. (iii) Although GPCRs are structurally similar, their native ligands are of vastly different structure and size, from small cationic amines to medium-sized proteins. In this review, we discuss key features of our GPCR models and show that they are consistent with general principles of protein structure. In addition, we compare the models with the most recently published electron microscopy data for rhodopsin [3,15] and with mutagenesis studies of cationic amine receptors.

Atomic-resolution models of GPCRs calculated by distance geometry with hydrogen bonding constraints

The approach developed to construct the models described here is based upon the presence of numerous polar residues in the transmembrane segments of GPCRs. It is known that water-inaccessible polar groups of proteins have a strong tendency to form H-bonds [18]. In transmembrane α-helices, backbone peptide groups are already paired, while the polar side-chains must interact with each other to form intra- or interhelical H-bonds. The candidate H-bonding pairs can be identified from the analysis of sequence alignments as polar residues that appear and disappear simultaneously in various GPCRs and by using approximate receptor models to exclude all spatially distant residues from the list of possible correlations. H-bonds thus identified can be applied as distance constraints for the packing of the transmembrane α-helices, using the distance geometry algorithm. Since the rhodopsin-like GPCRs share a common 3D structure of the transmembrane domain, the side-chain H-bonds from many different GPCRs can be combined in order to increase the number of simultaneously applied constraints and to calculate an 'average' 7-α-bundle structure. This average structure is subsequently used to restrain the positions of the transmembrane helices in the calculation of the 7-α-bundle for 'specific' GPCRs.

The computational procedure, described elsewhere [16], was organized as an iterative refinement with evolving constraints that begins with an initial, approximate model of the α-bundle and continues until each buried polar side-chain of each of the 410 GPCRs considered participates in at least one hydrogen bond in the final structure. Each iteration of the refinement included (i) examination of the structures calculated in the previous iteration for additional or alternative H-bonds, for correlations in sequence alignments, and for structural flaws, such as buried polar groups lacking any H-bonds, violations of constraints, α-helices multiply curved by contradictory constraints or loosely packed because of insufficient constraints, or hindrances or holes produced by incorrectly packed side-chains; (ii) modification of distance and angle constraints (H-bonds and conformers of side-chains) to correct detected flaws and to increase the number of simultaneously formed H-bonds; and (iii) distance geometry calculations with the modified constraints using the program DIANA [19]. The analysis of calculated structures (step (i)) was performed using the programs ADJUST [16] and QUANTA (Molecular Simulations Inc.). The constraints and the corresponding α-bundle structure simultaneously evolved during the refinement. The search for the proper side-chain conformers and H-bonds was guided primarily by correlations in multiple sequence alignments of GPCRs.

The final 'average' 7-α-bundle structure, obtained after >500 iterations of the refinement procedure, differs significantly from the initial structure: the rmsd of C^{α} atoms of the initial and final structures was ∼4 Å. In the final model, each water-inaccessible polar side-chain of all 410 sequences considered (collectively, >20000 side-chains) participates in at least 1 H-bond. This 'saturation of H-bonding potential' criterion was very sensitive to errors during the refinement. The transmembrane segments of individual GPCRs are hydrophobic and contain less than 30% polar residues (Figure 1), but when 410 different amino acid sequences are simultaneously considered, all interhelical contacts within the α-bundle are 'labeled' by polar side-chains forming intramolecular H-bonds, usually in a group of related receptors. Displacement of α-helices from their correct positions breaks some

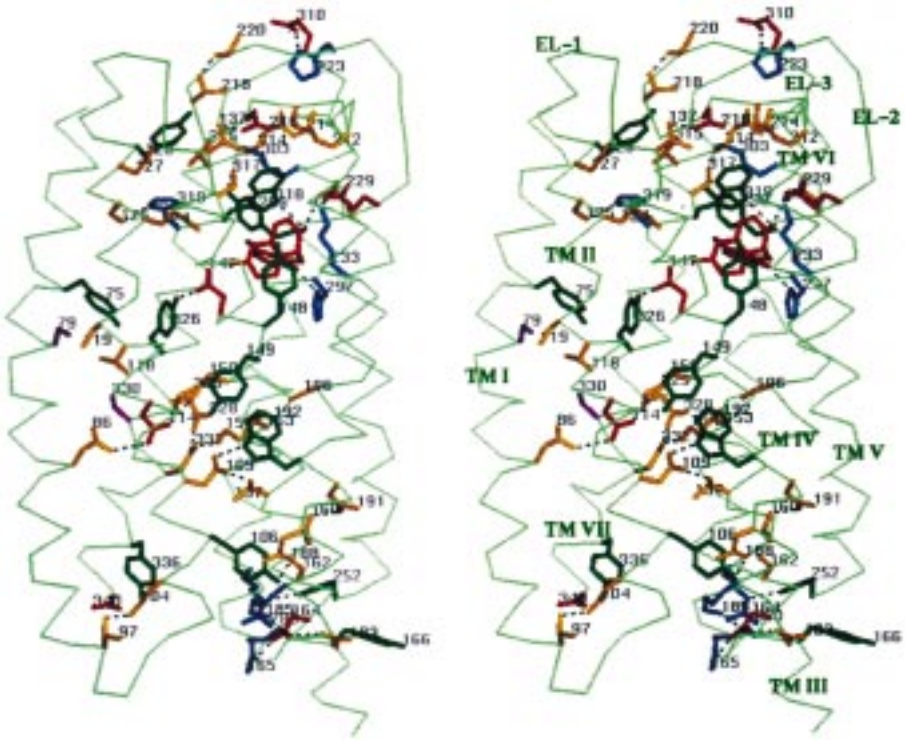

Figure 1. 'Saturation of H-bond potential' of polar residues in the μ-opioid receptor model. The color indicates residue type: white, aliphatic (Ala, Pro, Val, Leu, Ile); green, aromatic (Phe, Tyr, Trp); magenta, sulfur-containing (Cys, Met); yellow, polar (Ser, Thr, Asn, Gln); red, acidic (Asp, Glu); blue, basic (Lys, Arg). The μ-selective agonist (−)morphine is shown in orange. H-bonds are indicated by dashed lines. H-bonds with deviations from standard donor–acceptor distances >0.3 Å, H-bonds formed by Cys and N^{ϵ} atoms of His residues, and main-chain–side-chain H-bonds are not shown. The residue numbers correspond to the μ-opioid receptor sequence.

H-bonds, producing unpaired polar side-chains within the lipid bilayer in tens or hundreds of GPCRs.

We have tested the 'average' atomic structure of the α-bundle by using it as a template to calculate the transmembrane domains of 26 different GPCRs from eight remotely related subfamilies: vertebrate and invertebrate opsins, cationic amine, melatonin, opioid, chemokine, purine, and glycoprotein hormone receptors (Table 1, Figure 2). The models were generated by distance geometry using the H-bonds applicable for each specific protein (Figure 1), while using the 'average' transmembrane structure to restrain the spatial positions of the helices. In addition, we have calculated the transmembrane domains of Duffy erythrocyte antigen and squid retinochrome, two proteins that have detectable sequence homology with GPCRs, but perform different functions: retinochrome restores the pool of 11-*cis* retinal in some invertebrates through all-*trans*→11-*cis* photoisomerization [20], while the Duffy erythrocyte antigen serves as a 'sink' for various chemokines [21]. Thus, both proteins share common ligands with their GPCR counterparts, rhodopsins and chemokine receptors, respectively. The models of opsins, cationic amine, melatonin, opioid, and purine receptors and retinochrome were tested for complementarity to the corresponding small, rigid ligands shown in Table 1. It must be emphasized that the models of different GPCRs are not completely identical. Changes in side-chain volumes and interhelical H-bonds cause some shifts of entire helices and small variations in their tilts and curvatures. Sometimes, the appearance of a proline residue, usually close to the extracellular side of the α-bundle, induces additional kinks in the helices. Moreover, the conformations of homologous side-chains can vary in different receptors to provide optimum packing. These differences between the various GPCRs considered, clearly revealed in the iterative distance geometry approach, would not be reproduced by standard 'modeling by homology' procedures.

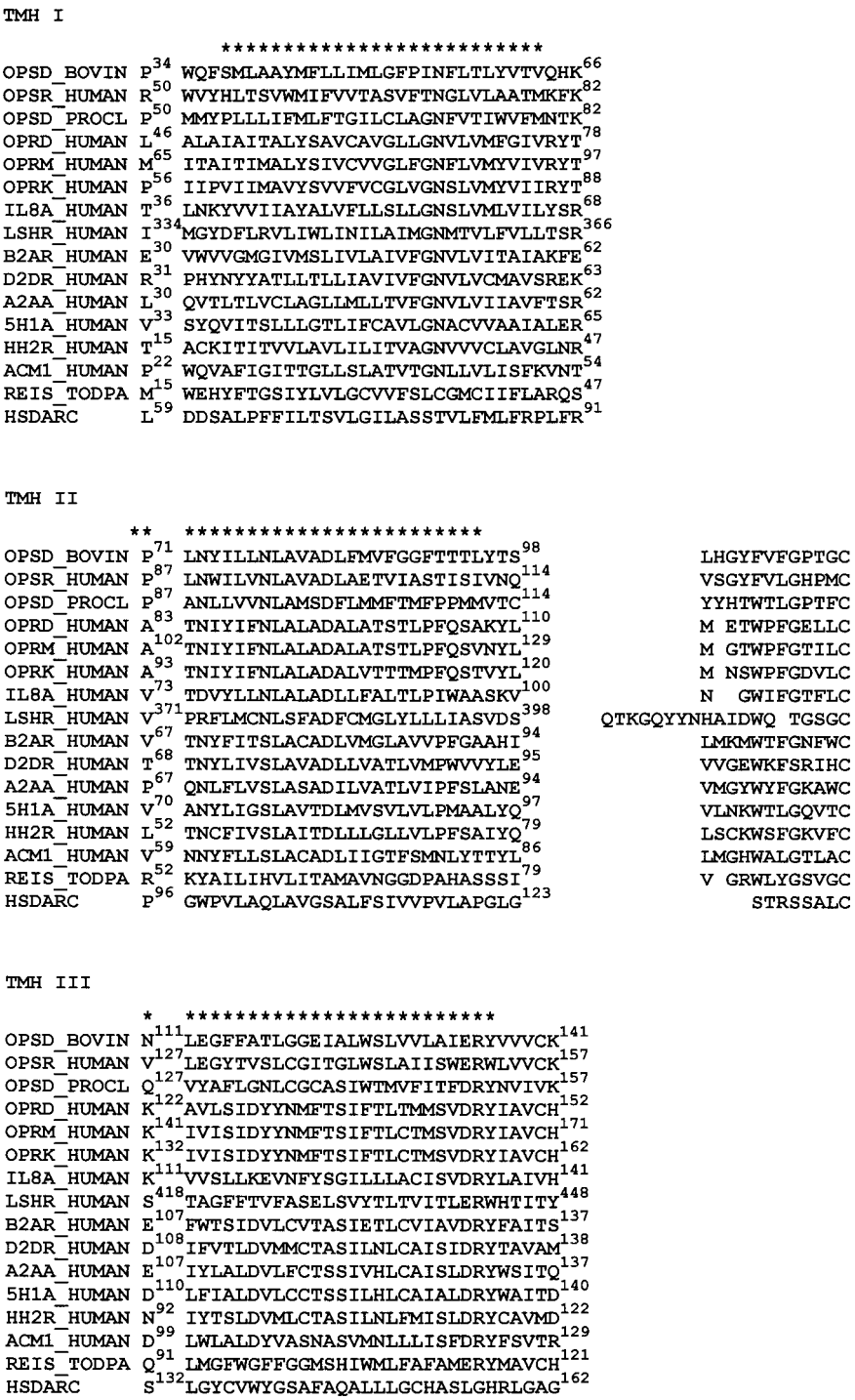

Figure 2. Alignment of amino acid sequences of bovine, red cone, and crayfish opsins, μ-, δ-, and κ-opioid, interleukin-8A, lutropin/choriogonadotropin hormone, β_2- and α_{2A}-adrenergic, D_{2A} dopamine, $5HT_{1A}$ serotonin, H_2 histamine, m_1 muscarinic receptors, squid retinochrome, and Duffy erythrocyte antigen (sequence identifiers are shown in Table 1). The string of asterisks above each transmembrane helix (TMH) indicates the 26-residue transmembrane segments identified by Baldwin [5] and used for 'generic' numbering. In this numbering system, V:3, as an example, designates the third residue of the 26-residue TMH V segment defined by Baldwin. As indicated in the figure, the transmembrane segments determined in our studies typically are longer. All Arabic numbers listed correspond to the individual sequences. N- and C-terminal segments and intracellular loops are omitted. Alignments of TMH I of squid retinochrome and TMHs I, II, III, and V of Duffy antigen were obtained during distance geometry calculations of their transmembrane domains to satisfy the H-bond potential of the polar residues in the helices. Alignment of the extracellular loop sequences was done using the ends of the transmembrane helices and conserved cysteines as 'reference points'.

```
TMH IV

                  **************************
OPSD_BOVIN E150NHAIMGVAFTWVMALACAAPPLVGWSRY178       IPEG MQCSCGIDYYTPHEETN
OPSR_HUMAN A166KLAIVGIAFSWIWSAVWTAPPIFGWSRY194       WPHG LKTSCGPDVFSGSSYPG
OPSD_PROCL T166KKASLWILTIWVLSITWCIAPFFGWNRY194       VPEG NLTGCGTDYLSED  IL
OPRD_HUMAN P162AKAKLINICIWVLASGVGVPIMVMAVTR190       PRDG  AVVCMLQFPSPSW YW
OPRM_HUMAN P181RNAKIINVCNWILSSAIGLPVMFMATTK209       YRQG  SIDCTLTFSHPTW YW
OPRK_HUMAN P172RNAKIINVCNWLLSSSVGVSAIVLGGTK200       VREDVDVIECSLQFPDDDYSWW
IL8A_HUMAN R150HLVKFVCLGCWGLSMNLSLPFFLFRQAY178       HPNN SSPVCYEVLGNDTAKW
LSHR_HUMAN L458RHAILIMLGGWLFSSLIAMLPLVGVSNY486         MK  VSICFPMDVETT
B2AR_HUMAN K147NKARVIILMVWIVSGLTSFLPIQMHWYR175 ATHQEAINCYANETCCDFFT
D2DR_HUMAN K149RRVTVMISIVWVLSFTISCPLLFGLNNA177          DQNECIIA
A2AA_HUMAN P147RRIKAIIITVWVISAVISFPPLISIEKK175     GGGGPQPAEPRCEIND
5H1A_HUMAN T149PRPRALISLTWLIGFLISIPPMLGWRTP177        EDRSDPDACTISK
HH2R_HUMAN P132VRVAISLVLIWVISITLSFLSIHLGWNS160   RNETSKGNHTTSKCKVQV
ACM1_HUMAN P148RRAALMIGLAWLVSFVLWAPAILFWQYL167      VGERTVLAGQCYIQFLS
REIS_TODPA S130VYYSIIVGLMYTFGTFWATMPLLGWASY158       GLEV HGTSCTINYSVSD  ES
HSDARC     P165GLTLGLTVGIWGVAALLTLPVTLASGAS193            GGLCTLIYSTE

TMH V

                   **************************
OPSD_BOVIN N200ESFVIYMFVVHFIIPLIVIFFCY223
OPSR_HUMAN V216QSYMIVLMVTCCIIPLAIIMLCY239
OPSD_PROCL S214RSYLYDYSTWVYYLPLLPIYCYV237
OPRD_HUMAN D210TVTKICVFLFAFVVPILIITVCY233
OPRM_HUMAN E229NLVKICVFIFAFIMPVLIITVCY252
OPRK_HUMAN E223LFMKICVFIFAFVIPVLIIIVCY246
IL8A_HUMAN R199MVLRILPHTFGFIVPLFVMLFCY222
LSHR_HUMAN L501SQVYILTILILNVVAFFIICACY524
B2AR_HUMAN N196QAYAIASSIVSFYVPLVIMVFVY219
D2DR_HUMAN N186PAFVVYSSIVSFYVPFIVTLLVY209
A2AA_HUMAN Q193KWYVISSCIGSFFAPCLIMILVY216
5H1A_HUMAN D191HGYTIYSTFGAFYIPLLLMLVLY214
HH2R_HUMAN N179EVYGLVDGLVTFYLPLLIMCITY202
ACM1_HUMAN Q185PIITFGTAMAAFYLPVTVMCTLY208
REIS_TODPA Y178QSYVFFLAIFSFIFPMVSGWYAI201
HSDARC     L205KALQATHTVACLAIFVLLPLGLF228

TMH VI

                   **************************
OPSD_BOVIN E247KEVTRMVIIMVIAFLICWLPYAGVAFYIFT277   HQGSD           FG
OPSR_HUMAN E263KEVTRMVVVMIFAYCVCWGPYTFFACFAAA293   NPGYA           FH
OPSD_PROCL E273CRLAKIAMTTVALWFIAWTPYLLINWVGMF303   ARSY            LS
OPRD_HUMAN L256RRITRMVLVVVGAFVVCWAPIHIFVIVWTL286   VDIDRRDP        LV
OPRM_HUMAN L275RRITRMVLVVVAVFIVCWTPIHIYVIIKAL305   VTIPETT         FQ
OPRK_HUMAN L269RRITRLVLVVVAVFVVCWTPIHIFILVEAL299   GSTSHST         AA
IL8A_HUMAN K237HRAMRVIFAVVLIFLLCWLPYNLVLLADTL267   MRTQVI QETCERRNNI
LSHR_HUMAN D542TKIAKKMAILIFTDFTCMAPISFFAISAAF572   KVPLI           TV
B2AR_HUMAN E268HKALKTLGIIMGTFTLCWLPFFIVNIVHVI298   QDNL            IR
D2DR_HUMAN E368KKATQMLAIVLGVFIICWLPFFITHILNIH398   CDC            NIP
A2AA_HUMAN E369KRFTFVLAVVIGVFVVCWFPFFFTYTLTAV399   GCS             VP
5H1A_HUMAN E339RKTVKTLGIIMGTFILCWLPFFIVALVLPF369   CESS          CHMP
HH2R_HUMAN E229HKATVTLAAVMGAFIICWFPYFTAFVYRGL259   RGDD           AIN
ACM1_HUMAN E360KKAARTLSAILLAFILTWTPYNIMVLVSTF390   CKDC            VP
REIS_TODPA E225EQLTALAGAFILISLISWSGFGYVAIYSAL255   THGGAQ          LS
HSDARC     L237GMGPGPWMNILWAWFIFWWPHGVVLGLDFL267   VRSKLLLLSTCLAQQAL
```

Figure 2. (continued).

```
TMH VII
                  *************************
OPSD_BOVIN P285IFMTIPAFFAKTSAVYNPVIYIMMN310
OPSR_HUMAN P301LMAALPAYFAKSATIYNPVIYVFMN326
OPSD_PROCL P310VYTIWGYVFAKANAVYNPIVYAISH335
OPRD_HUMAN V297AALHLCIALGYANSSLNPVLYAFLD322
OPRM_HUMAN T315VSWHFCIALGYTNSCLNPVLYAFLD340
OPRK_HUMAN L309SSYYFCIALGYTNSCLNPILYAFLD334
IL8A_HUMAN G284RALDATEILGFLHSCLNPIIYAFIG309
LSHR_HUMAN T580NSKVLLVLFYPINSCANPFLYAIFT605
B2AR_HUMAN K305EVYILLNWIGYVNSGFNPLIYCRSP330
D2DR_HUMAN P405VLYSAFTWLGYVNSAVNPIIYTTFN430
A2AA_HUMAN R405TLFKFFFWFGYCNSSLNPVIYTIFN430
5H1A_HUMAN T378LLGAIINWLGYSNSLLNPVIYAYFN403
HH2R_HUMAN E267VLEAIVLWLGYANSALNPILYAALN292
ACM1_HUMAN E397TLWELGYWLCYVNSTINPMCYALCN422
REIS_TODPA H264LRGHVPPIMSKTGCALFPLLIFLLT289
HSDARC     D285LLLNLAEALAILHCVATPLLLALFC310
```

Figure 2. (continued).

Driving forces of GPCR folding

Clustering of groups with similar polarities and formation of H-bonds

The most general feature of protein structure is the formation of clusters of groups with similar polarities, which can be arbitrarily divided into highly polar (hydroxyl, peptide groups, etc.), intermediate polarity (sulfur-containing and aromatic), and nonpolar (aliphatic) groups. The formation of such clusters is energetically favorable, since chemically similar compounds are more soluble in each other. The tendency of nonpolar residues in proteins to be shielded from water (and therefore to be clustered together in the hydrophobic core), which is usually treated as the main principle of protein structure [22], or the major driving force of protein folding [23], can be considered to be a specific case of this more general 'clustering by polarity' rule, which governs protein folding, protein–lipid interactions (as discussed below), and the formation of bilayers and micelles.

In proteins, clustering by polarity appears, first of all, as hydrogen bonding of the polar backbone (~ -1.3 kcal/mol per H-bond in an α-helix [24]) and formation of hydrogen bonds between side-chains (up to -0.5 kcal/mol per H-bond between two flexible side-chains in water [25,26]). A striking example of clustering by polarity is the spatial distribution of 43 conserved GPCR residues that form a continuous 'minicore' inside the α-bundle composed of several layers with different polarities. The first layer, in the middle of the transmembrane domain (Figure 3), consists mainly of polar H-bonded residues that connect helices I, II, III, and VII (Asn^{55}(I:18), Asp^{83}(II:14), Ser^{124}(III:14), Asn^{298}(VII:13), Ser^{299}(VII:14), Asn^{302}(VII:17), and Tyr^{306}(VII:21)) and helices II and IV (Asn^{78}(II:4) ... Trp^{161}(IV:11)). In different receptors, this H-bond network can be extended by additional polar residues in positions I:17, II:11, II:15, II:17, II:18, III:10, VII:15 (for example, in red cone opsin, these additional residues are Thr^{70}(I:17), Glu^{102}(II:17), Thr^{103}(II:18), and Cys^{136}(III:10)). The next layer, closer to the intracellular side, consists of 13 tightly packed, nonpolar aliphatic side-chains from all seven helices (Figure 3). The third layer consists of two clusters of polar side-chains at the intracellular surface of the receptor – Asn^{73}(II:4)-Asn^{310}(VII:25) and Ser^{132}(III:22)-Glu^{134}(II:24)-Arg^{135}(III:25)-Tyr^{136}(III:26)-Tyr^{233}(V: 22) (at the bottom of Figure 3). At the opposite, extracellular side of the receptor, the cluster of aromatic and sulfur-containing residues (Phe^{212}(V:11)-Phe^{261}(VI:12)-Cys^{264}(VI:15)-Trp^{265}(VI:16)-Tyr^{268}(V I:19)-Phe^{294}(VII:9)) and two residues conserved within subfamilies of GPCRs (for example, Met^{44}(I:7), Lys^{296}(VII:11) in opsins) form a layer near the ligand-binding pocket.

A number of additional polar clusters appear only in small groups of GPCRs. For example, the H-bonded Glu^{122}-His^{211} (III:12-V:10) pair is present only in vertebrate rhodopsins (Figure 4). The spatial distribution of various groups around this pair has the appearance of a polarity or solubility gradient, in which the most polar residues are shielded from nonpolar aliphatic ones by a shell of aromatic and sulfur-containing side-chains.

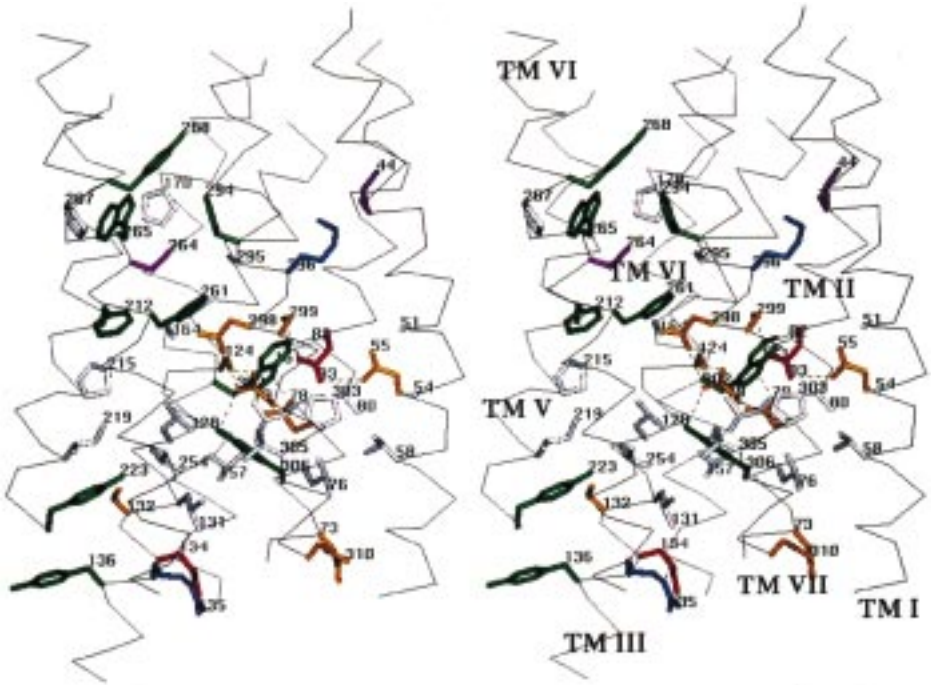

Figure 3. The evolutionarily conserved domain of GPCRs, depicted as the bovine rhodopsin structure with six residues replaced by more conserved ones (I56G, T58V, A124S, A132S, S298N, and A299S). The set of 43 conserved residues was identified from the analysis of sequence alignments of several GPCR subfamilies [16]. Colors are as in Figure 1. H-bonds are indicated by dashed lines. Residue numbers correspond to the bovine rhodopsin sequence.

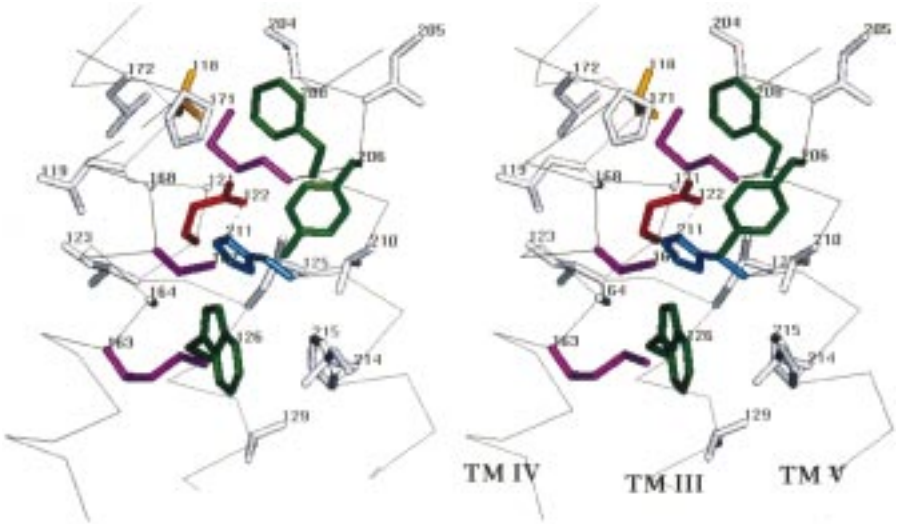

Figure 4. The Glu^{122}-His^{211} pair and its surroundings in bovine rhodopsin. Colors are as in Figure 1. H-bonds are indicated by dashed lines. Residue numbers correspond to the bovine rhodopsin sequence.

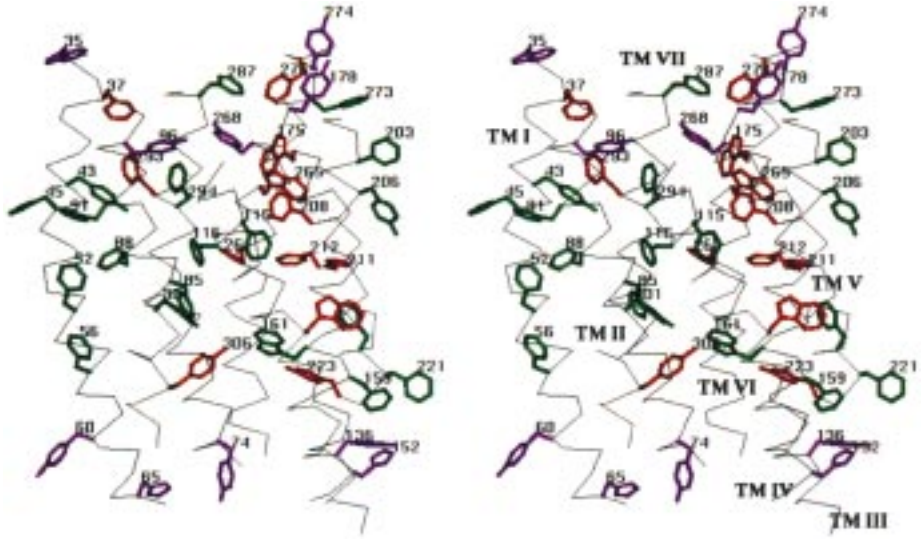

Figure 5. Spatial arrangement of aromatic (Phe, Tyr, Trp, and His) residues in the bovine rhodopsin model. The residues are classified as buried within the transmembrane α-bundle (orange), exposed to the lipid acyl chains (green), and exposed to the interfacial area of the bilayer, formed by lipid head groups (magenta). Residue numbers correspond to the bovine rhodopsin sequence.

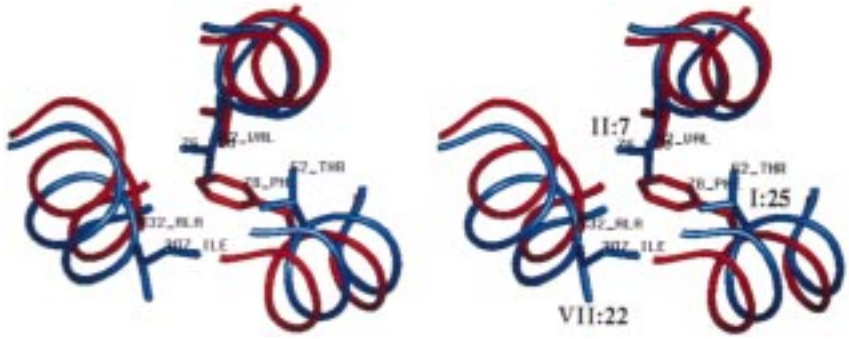

Figure 6. An example of correlated replacements of nonpolar residues in bovine (blue) and crayfish (red) rhodopsins. Residue numbers of both receptors are indicated.

The GPCR models also form spectacular clusters of aromatic side-chains, which can be found either at the outer (lipid-facing) surface or buried within the transmembrane domain (Figure 5). The lipid-facing Phe 45, 52, 56, 85, 88, 115, 116, and Trp^{161} residues at the external surfaces of helices I, II, III, and IV in bovine rhodopsin fit together as pieces of a jigsaw puzzle, creating a continuous sheet of closely packed aromatic side-chains (Figure 5). At the same time, helices III, IV, V, VI, and VII are linked together through a ribbon of lipid-inaccessible, interacting aromatic side-chains of Trp^{126}, Tyr^{206}, Phe^{208}, His^{211}, Phe^{212}, Tyr^{261}, and Trp^{265} (Figure 5, a part of this ribbon is also seen in Figure 4). In bovine rhodopsin, the side-chains of Tyr^{43}, Tyr^{206}, Tyr^{301}, and Trp^{161} face the lipid environment, but their polar groups form H-bonds either with main-chain carbonyls (all three tyrosines) or with other polar side-chains (Asn^{78}-Trp^{161} pair).

'Solubility forces' are equally important for protein–lipid interactions. For example, the lipid-facing aromatic clusters (Figure 5) may increase the solubility of rhodopsin in photoreceptor membranes, which have an unusually high content of lipids with unsaturated fatty acids [27]. The protein–lipid interactions cause anisotropy of polarity of two different types. First, the interior of GPCRs is more polar than their lipid-facing surfaces (Figures 1, 3 and 4), as is normally observed in α-helical transmembrane proteins [28]. Secondly, the polarities of the lipid-facing side-chains have an anisotropic distribution in the direction perpendicular to the membrane plane to

match nonpolar tails and polar head groups of lipids. For example, the lipid-facing surface of the transmembrane α-bundle in bovine rhodopsin consists of aliphatic and Phe residues in the middle of the bilayer, and weakly polar aromatic Tyr, Trp, and His residues closer to the interfacial area (Figure 5). Similar, layer-like, anisotropic distributions of side-chains with different polarities are found in all structures of transmembrane proteins, including α-bundles of bacterial photoreaction centers [29], bacteriorhodopsin [30,31], sodium channels [32], cytochrome c oxidase [33], cytochrome b/c1 complex [34], β-barrels of porins [35] and maltoporin, and right-handed π-helices (head-to-head dimers) of gramicidin A [36]. The interfacial region is especially abundant in Trp residues. The solubility of 3-methyl-indole, the structural equivalent of the Trp side-chain, is significantly higher in the interfacial region of membranes than in water or in cyclohexane (which approximates the membrane core) [37,38]. Remarkably, the entire structure of gramicidin A depends on such solubility effects: in isotropic organic solvents, this peptide forms various double π-helices with uniformly distributed Val and Trp residues at the surface [39], instead of the head-to-head dimers observed in micelles, in which the Trp side-chains are concentrated at the ends of the π-helix, at the water–detergent interface.

Side-chain packing

The geometrical packing of side-chains is another factor that is important for the stability of proteins [40]. All of our calculated GPCR structures are tightly packed except for a few cavities, formed mostly by polar groups, that can be filled by water, sodium ion, or ligands. The close packing of side-chains leads to correlated replacements of residues in order to preserve the structural integrity of the transmembrane core. The appearance of a bulky (especially aromatic) side-chain in the core usually requires a concomitant decrease of volume in several surrounding side-chains. For example, the appearance of the Phe^{78} side-chain in crayfish rhodopsin, in place of Thr^{62}(I:25), present in bovine rhodopsin, is correlated with $Leu^{76}\rightarrow Val^{91}$(II:7) and $Ile^{307}\rightarrow Ala^{322}$(VII:22) replacements (Figure 6). Occasionally, one aromatic side-chain spatially substitutes for another, even if their sequence positions differ. For example, Tyr(I:7), present in most peptide GPCRs, is spatially substituted by Trp(VII:8) in most cationic amine receptors. Comparison of any two remotely related GPCRs reveals a multitude of such correlated replacements throughout the transmembrane core. This topic is considered further below.

Covalent cross-linking

The calculation of the 'average' structure of the transmembrane domain presented the opportunity to explore the formation of disulfide bonds in the GPCR family. This was done by searching for pairs of sufficiently close cysteines in all 410 GPCRs considered, using the program ADJUST [16]. As a result, 16 different pairs of spatially proximate cysteines, which collectively are present in 103 different GPCRs, were detected (Table 2). All these pairs can have mutual orientations of Cys side-chains appropriate for the formation of disulfide bonds. As shown by site-directed mutagenesis, all spatially close cysteine pairs form disulfide bonds in proteins, even when inappropriately arranged [41,42]. Thus, each of the 16 cysteine pairs detected can be expected to form a disulfide bond when present in GPCRs. To determine whether the disulfide bonds are mutually compatible, all 16 putative disulfides were simultaneously included in the calculations of the average model as supplementary constraints. This increased the structural compactness of the α-bundle without causing violations of the other constraints. Some of the proposed disulfide bonds were tested further by incorporating them into models of specific GPCRs, such as Cys^{228}-Cys^{278} (V:12-VI:13) in red cone opsin, Cys^{117}-Cys^{201} (III:11-V:7) in the α_2-adrenergic receptor, Cys^{130}-Cys^{157} (III:20-IV:7) in the IL-8A receptor and similar cysteines in the IL-8B receptor, Cys^{138}-Cys^{184} (III:12-IV:18) in crayfish rhodopsin, Cys^{132}-Cys^{217} (III:26-V:21) in the ATP P_{2U} receptor and the corresponding Cys^{135}-Cys^{216} (III:26-V:21) cysteine pair in a chemokine receptor from *Herpesvirus saimiri*, and Cys^{95}-Cys^{310} (II:1-VII:25) in Duffy antigen. Again, these disulfide bonds were found to be consistent with all the other constraints in the specific GPCRs.

Interestingly, two opsins (X65877, P28678), three melanocortin receptors (B46647, P33033, P32244), and one high-affinity interleukin-8 receptor (P25024) have one cysteine in helix III (in position III:12, III:16, or III:20) and two proximal cysteines in helix IV (IV:17 and IV:18, IV:13 and IV:14, or IV:7 and IV:10, respectively). In these cases, the Cys from helix III can form a disulfide bond with either of the two corresponding cysteines from helix IV. The Cys(III:12)-Cys(IV:18), Cys(III:16)-Cys(IV:14),

Table 2. Proposed interhelical disulfide bonds in the transmembrane domain of GPCRs

Pairs of residues	Types and number of receptors
I:14-VII:15	2 opsins
II:16-III:6	3 opsins
II:18-VII:15	3 opsins, 3 cholecystokinin, 3 C5a anaphylatoxin receptors
II:21-VII:8	1 angiotensin II, 1 galanin receptor
III:8-V:6	7 melanocortin receptors
III:11-V:7	9 α_2-adrenergic receptors
III:12-IV:17	2 opsins
III:12-IV:18	4 opsins
III:16-IV:13	5 bradykinin, 3 melanocortin receptors
III:16-IV:14	11 melanocortin receptors
III:19-V:17	5 endothelin receptors
III:20-IV:7	17 angiotensin, 8 high-affinity interleukin-8 receptors
III:20-IV:10	1 high-affinity interleukin-8 receptor
III:26-V:21	2 oxytocin, 6 FMLP-related receptors
IV:18-V:10	4 cone opsins
V:11-VI:13	10 cone opsins

and Cys(III:20)-Cys(IV:7) disulfide bonds are more consistent with other constraints incorporated in the 'average' model. However, the alternative disulfide bonds can be formed by thiol–disulfide exchange, if the position of helix III relative to helix IV changes slightly, for example during activation of these receptors. This hypothesis can be experimentally tested by mutagenesis.

Another interesting feature of the detected disulfide bonds relates to their spatial locations in the α-bundle. Most of the disulfides appear in regions of the transmembrane domain that have a relatively small number of interhelical H-bonds, i.e. between helices III and IV, III and V, and V and VI. Apparently, these disulfide bonds serve to stabilize the α-bundle when other structure-stabilizing factors, such as interhelical H-bonds, are insufficient.

Metal-binding clusters formed by Cys and His residues [43] represent another type of natural cross-link in proteins. A search for such clusters in the 410 sequences examined reveals that only squid retinochrome has four spatially close residues in the transmembrane domain – His^{18}(I:0), His^{74}(II:24), His^{264}(VII:0) and His^{268}(VII:4) – that have the tetrahedral geometry appropriate to form a Zn^{2+}-binding site (Figure 7C). The formation of the Zn^{2+}-binding site is facilitated by the appearance of an additional proline residue, Pro^{271}(VII:7), in retinochrome, which disrupts the N-terminal part of helix VII, allowing the formation of a short 3_{10}-helix (the appearance of a 3_{10}-helix is usually observed between two histidines, in the i and $i+4$ positions of an α-helix, that form a metal-binding site, as, for example, in Zn-fingers (PDB file: 1zaa)). The formation of a metal-binding cluster may be related to the unusually short N-terminus in retinochrome (14 residues, compared with 33 residues in bovine rhodopsin), which may be insufficient to stabilize the receptor structure in the region near the extracellular ends of helices I, II, and VII. Therefore, the metal-binding center may play a structure-stabilizing role. Moreover, one of these histidines (His^{268}(VII:4)) forms an H-bond with Asp^{71}(II:21), a counterion of the protonated all-*trans* retinal Schiff's base (SB) in the retinochrome model (see below). Thus, metal binding to the histidine cluster may contribute to regulation of spectral tuning of the pigment, retinal photoisomerization, or hydrolysis of the SB.

Evolution of GPCR structures

Relatedness of GPCRs and bacterial light-sensitive proteins

The experimental structure of bacteriorhodopsin (PDB file: 2brd, Reference 31) and our independently derived rhodopsin model (PDB file: 1boj) differ in

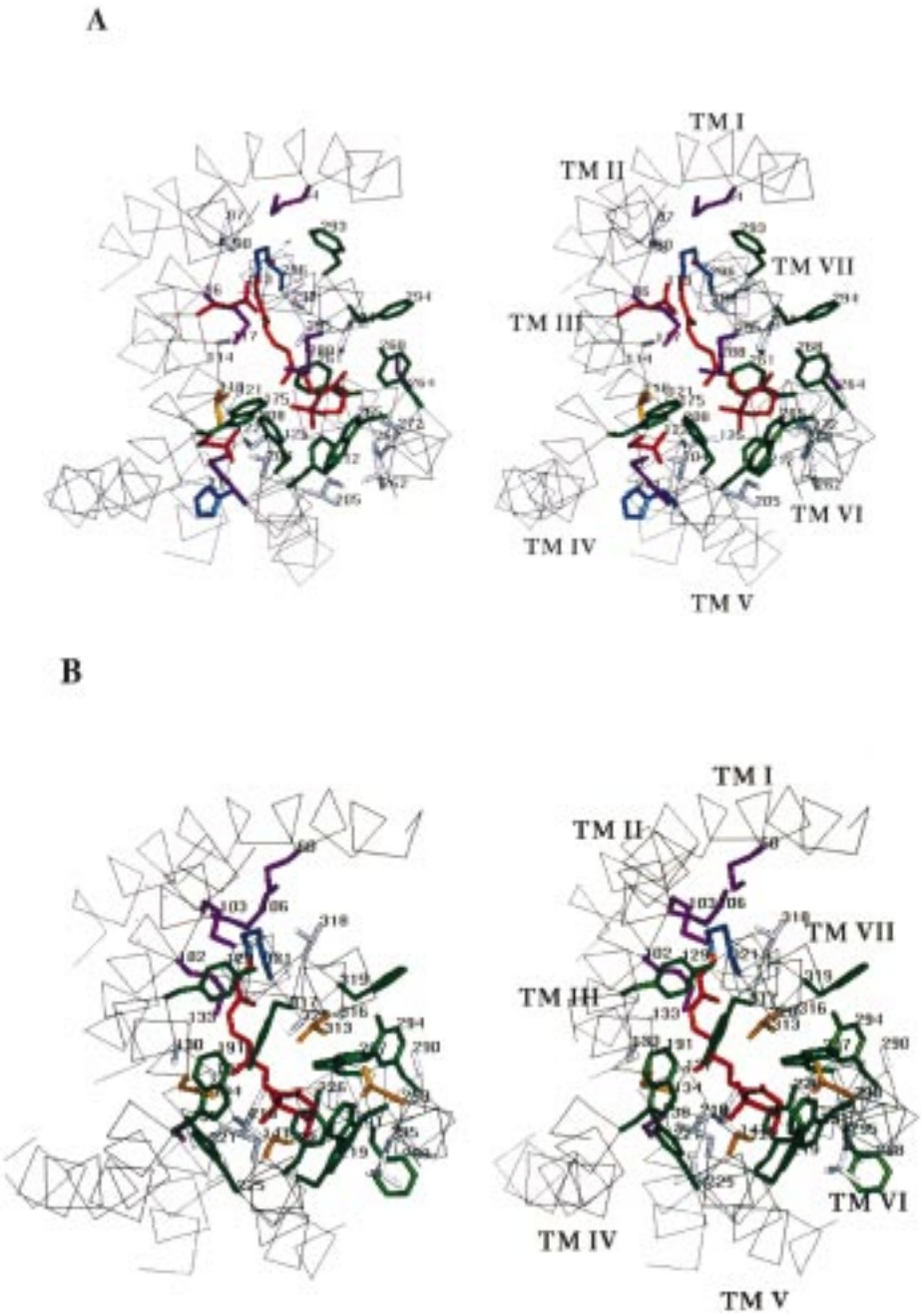

Figure 7. Binding pockets of 11-*cis* retinal in bovine rhodopsin (A), 3-hydroxy-11-*cis* retinal in crayfish rhodopsin (B), and all-*trans* retinal in squid retinochrome (C). Colors are as in Figure 1. A possible bound water molecule near the PSB in bovine rhodopsin is shown as a dotted red sphere in (A). Ligands are shown in orange.

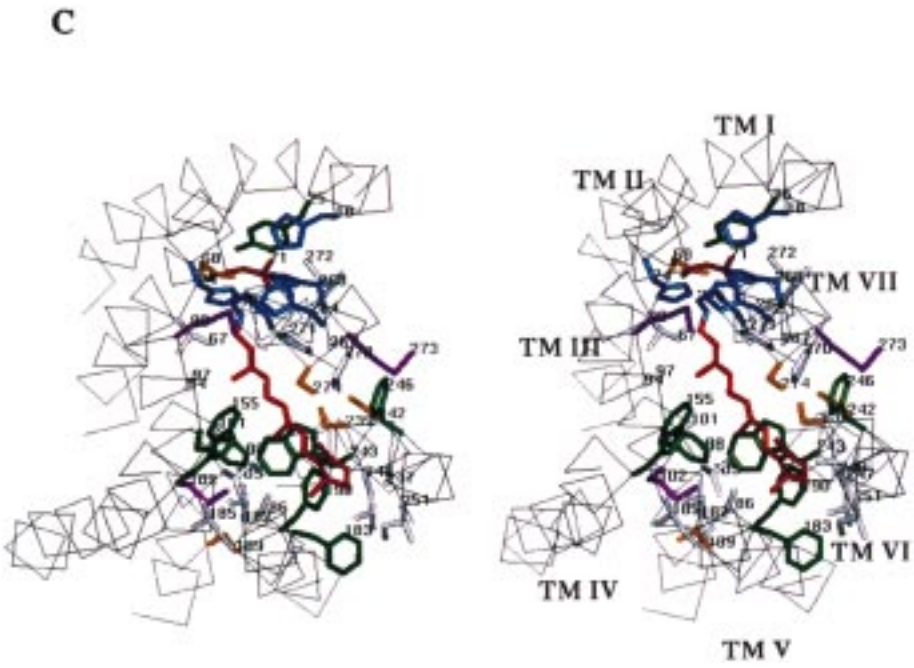

Figure 7. (continued).

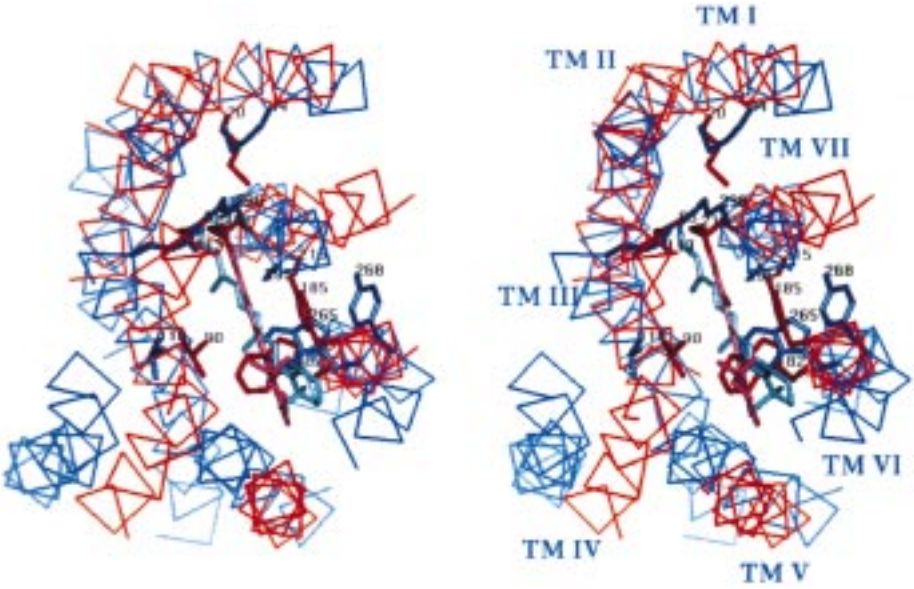

Figure 8. Superposition of the bovine rhodopsin model with bound all-*trans* retinal (PDB file: 1boj, blue) and the bacteriorhodopsin structure (PDB file: 2brd, Reference 31, red). Selected residues surrounding all-*trans* retinal are shown. The C^{α} atoms of helical segments 12–33, 41–61, 84–104, 108–123, 139–156, 167–187, and 207–227 of bacteriorhodopsin were superimposed with segments 36–57, 78–98, 112–132, 161–176, 202–219, 250–270, and 287–307 of bovine rhodopsin, respectively.

the positions of helices IV and V and in the tilts of helices II and III, consistent with EM data (Figure 8). Nonetheless, the optimum superposition of metarhodopsin II (complex with all-*trans* retinal) and bacteriorhodopsin models gives only a 2.9 Å rmsd for 140 common C^{α} atoms from all seven helices (Figure 8). Remarkably, this optimum superposition of C^{α} atoms simultaneously yields an excellent overlap of the retinylidene chromophore groups and the binding pockets in both proteins. Seven identical, or similar, functionally important residues in the retinal-binding pockets of rhodopsin and bacteriorhodopsin occupy spatially close positions (Figure 8): Lys^{296}(VII:11) and Lys^{216} which form the retinal SB; Glu^{113}(III:3) and Asp^{85} counterions of the SB; Met^{44}(I:7) and Met^{20} (whose S^{δ} atoms contact with the imine group of the SB); Thr^{118}(III:8) and Thr^{90}; Trp^{265}(VI:16) and Trp^{182}; Tyr^{268}(VI:19) and Tyr^{185}; and Ala^{295}(VII:10) and Ala^{215}. All these binding pocket residues are conserved in eukaryotic and bacterial photopigments, except for Met^{44}, Glu^{113}, and Thr^{118} of bovine rhodopsin (which are replaced in invertebrate rhodopsins) and Met^{20} and Asp^{85} of bacteriorhodopsin (which are replaced in bacterial halorhodopsins). The second acidic residue near the protonated SB in bacteriorhodopsin, Asp^{212}, is replaced by Ala^{292}(VII:7) in rhodopsin; the corresponding A292D (or A292E) replacement has been found in patients with congenital night blindness [44].

Other similar side-chains also spatially substitute for each other in the retinal-binding pocket, even though they come from different positions in the amino acid sequences. The side-chains of Phe^{293}(VII:8) and Tyr^{57}(II:25), of Phe^{276}(VI:27) and Trp^{189}(VI:23, one turn apart), and of Phe^{287}(VII:2) and Phe^{206}(VII:1, adjacent position) from rhodopsin and bacteriorhodopsin, respectively, spatially overlap and interact with the same groups of retinal. It is also noteworthy that Asp^{115} (helix IV), which is conserved in the bacteriorhodopsin family, spatially substitutes for Glu^{122} (helix III) which is near the β-ionone ring of 11-*cis* retinal in rhodopsin. The relatedness of these eukaryotic and bacterial light-sensitive proteins is not detectable from a comparison of their amino acid sequences [45] and can only be seen after superposition of their 3D structures, as is often observed for remotely related proteins with the same 3D folds and chemically similar ligands [46,47].

Coordinated replacements within the transmembrane domain

It is known that spatially proximate residues undergo coordinated changes in homologous protein families or, in other words, have similar 'conservation patterns' [48]. A comparison of receptor models from Table 1 reveals many such correlated replacements. The correlations arise when a residue significantly changes volume or polarity, which requires the concomitant replacement of several surrounding residues to maintain the structural integrity of the transmembrane core. The correlations usually are not pairwise, as is often assumed [49–52], but rather involve coordinated changes of groups of three and more residues, as in Figure 7, which was discussed above. Another interesting example of coordinated replacement is the appearance of a group of polar residues (Asn^{513}(V:11), Asp^{556}(VI:12), Met^{560}(VI:16) and Tyr/His^{590}(VII:10)) in the lutropin/choriogonadotropin receptor and other glycoprotein hormone receptors, in place of a 'sulfur–aromatic' cluster, Phe^{222}(V:11), Phe^{270}(VI:12), Trp^{274}(VI:16) and Gly^{307}(VII:10), present in most GPCRs (Figure 9). In glycoprotein hormone receptors, these polar residues form a network of H-bonds between helices V and VI that augments the conserved polar cluster of Asp II:14, Ser III:14, Asn VII:13, Asn VII:17, and Tyr VII:21 residues, which was described above.

The evolutionarily conserved domain of GPCRs

An additional example of 'coordinated behavior' in the GPCR family can be seen in the spatial arrangement of 43 evolutionarily conserved residues, which form a single continuous domain in the intracellular half of the α-bundle (Figure 3). Some of these residues are important for maintaining the appropriate structure of the 7-α-bundle, while others participate in signal transduction and/or form a regulatory sodium-binding site, which is present in many GPCRs [16]. The conserved residues II:14, III:14, III:24, III:25, V:22, VI:12, VI:16, VII:17, and VII:21 are involved in signal transduction, as identified by site-directed mutagenesis [53–63]. These conserved residues form a continuous path in our model of the transmembrane domain, starting from Phe^{261}(VI:12) and Trp^{265}(VI:16) situated at the bottom of the binding cavity, passing through the cluster of Asp^{83}(II:14), Ser^{124}(III:14) and Asn^{302}(VII:17) residues in the middle of the membrane, and ending at the Asp/Glu^{134}(III:24), Arg^{135}(III:25), Tyr^{223}(V:22)

and Tyr^{306}(VII:21) residues situated at the intracellular surface of the α-bundle. In the GPCR models, two conserved tyrosine residues (V:22 and VII:21) can form H-bonds either with residues from the central polar (as in Figure 3), or with residues at the intracellular surface (as in Figure 1), depending on their side-chain conformers. We have previously suggested that rotation of these tyrosines may occur during activation of GPCRs [16].

In the GPCR models, the largest cluster of conserved polar residues contains an empty space that can be filled by water or by a sodium ion coordinated with oxygens of the Asp^{95}(II:14), Asn^{131}(III:10), Ser^{135}(III:14), Ser^{311}(VII:14) and Asn^{314}(VII:17) side-chains, known to be involved in signal transduction [54,57,64–66] (Figure 10). The importance of Asp^{95}(II:14) for Na^+ binding has been shown by site-directed mutagenesis [55,67–70]. Remarkably, the cytoplasmic part of the proton-transfer pathway in bacteriorhodopsin (near Thr^{46}(II:14), Asp^{96}(III:14) and Phe^{219}(VII:14)) spatially coincides with the sodium-binding site of GPCRs after the superposition of rhodopsin and bacteriorhodopsin structures [16].

Structural similarities of extracellular loops

Although the transmembrane 7-α-helical domain plays a key role in ligand recognition and transduction, the importance of the extracellular loops for folding, ligand binding, and activation has also been demonstrated for many GPCRs, including amine receptors, opsins, 'peptide' (neurokinin, angiotensin, etc.), and 'protein' (chemokine, glycoprotein hormone) receptors [71–80]. The amino acid sequences and lengths of the loops and the N-terminal fragment can vary widely. Typically, extracellular loops 1 and 3 (EL-1 and EL-3) are relatively short and merely connect transmembrane helices, while the N-terminal segment and EL-2 are significantly longer (Figures 1 and 2). However, there are exceptions. For example, the N-terminal fragment is very short in purine receptors and EL-2 is truncated in melanocortin receptors, but is extremely long in a recently cloned orphan receptor [81]. Nevertheless, there are some clear indications of structural similarities of the loops, at least in some subfamilies of GPCRs. For example, EL-1 contains a characteristic conserved pattern, Gx(W/F)x(F/Y/L)GxxxC, and EL-2 has a conserved cysteine residue that forms a disulfide bond with a cysteine residue from the N-terminus of helix III (III:0).

Our recent attempts to model the three extracellular loops of opioid receptors [17] and red cone opsin (unpublished) indicate that corresponding loops form very similar structures throughout this set of receptors, despite low sequence identity and some differences in loop lengths in the opsin and opioid receptor subfamilies (Figure 2). Modeling of the loops was done using a modified version of the iterative distance geometry refinement employed for the transmembrane domain, but including a more precise identification of regular secondary structure based on analysis of hydrophobicity and variability patterns, correlations in sequence alignments, and maximization of the number of H-bonds and hydrophobic contacts in the loops. For example, the formation of a β-hairpin by the second extracellular loop, between helices IV and V (Figure 11), in all opioid receptors and vertebrate opsins can be inferred from a consistent $(i, i+2)$ pattern of polar residues in positions 214 and 216 (μ-opioid receptor numbering) and in positions 220 and 222, and nonpolar residues in positions 215, 219 and 221. These side-chains are segregated into polar and nonpolar clusters on the opposite sides of the β-hairpin. Moreover, analysis of multiple sequence alignments of GPCRs shows that there are correlated replacements of residues that are in register in this β-hairpin. Since the β-turn in the β-hairpin consists of an odd number of residues, the only possible standard type of β-turn is a type I with G1 β-bulge, or $\alpha_R\gamma_R\alpha_L$ motif [82]. This motif is very common in protein β-hairpins [82], and has been shown to be independently stable in aqueous solution [83] because, unlike the standard type I and II β-turns, the $\alpha_R\gamma_R\alpha_L$ turn is consistent with the direction of twist in β-structure [84]. In the μ-opioid receptor structure, this turn is additionally stabilized by H-bonds formed by the COO^- group of Asp^{216} with the main-chain NH group of Thr^{218}, and between side-chains of Thr^{218} and Thr^{220} (Figure 11).

In the calculated structures of μ-, δ-, and κ-opioid receptors and red cone opsin, the β-hairpin formed by EL-2 and two adjacent extracellular loops, EL-1 and EL-3, create an almost continuous, compact structure (Figure 1). The structural compactness of the extracellular domain, recently demonstrated by electron cryomicroscopy [3], is consistent with the presence of a disulfide bond connecting the N-terminus and EL-3 in chemokine, angiotensin, and endothelin receptors [85,86], an additional, nonconserved disulfide bond within EL-2 of β_2-adrenergic receptors [78], and with the simultaneous appearance of cysteine pairs (which probably form disulfides) in some extracellular GPCR

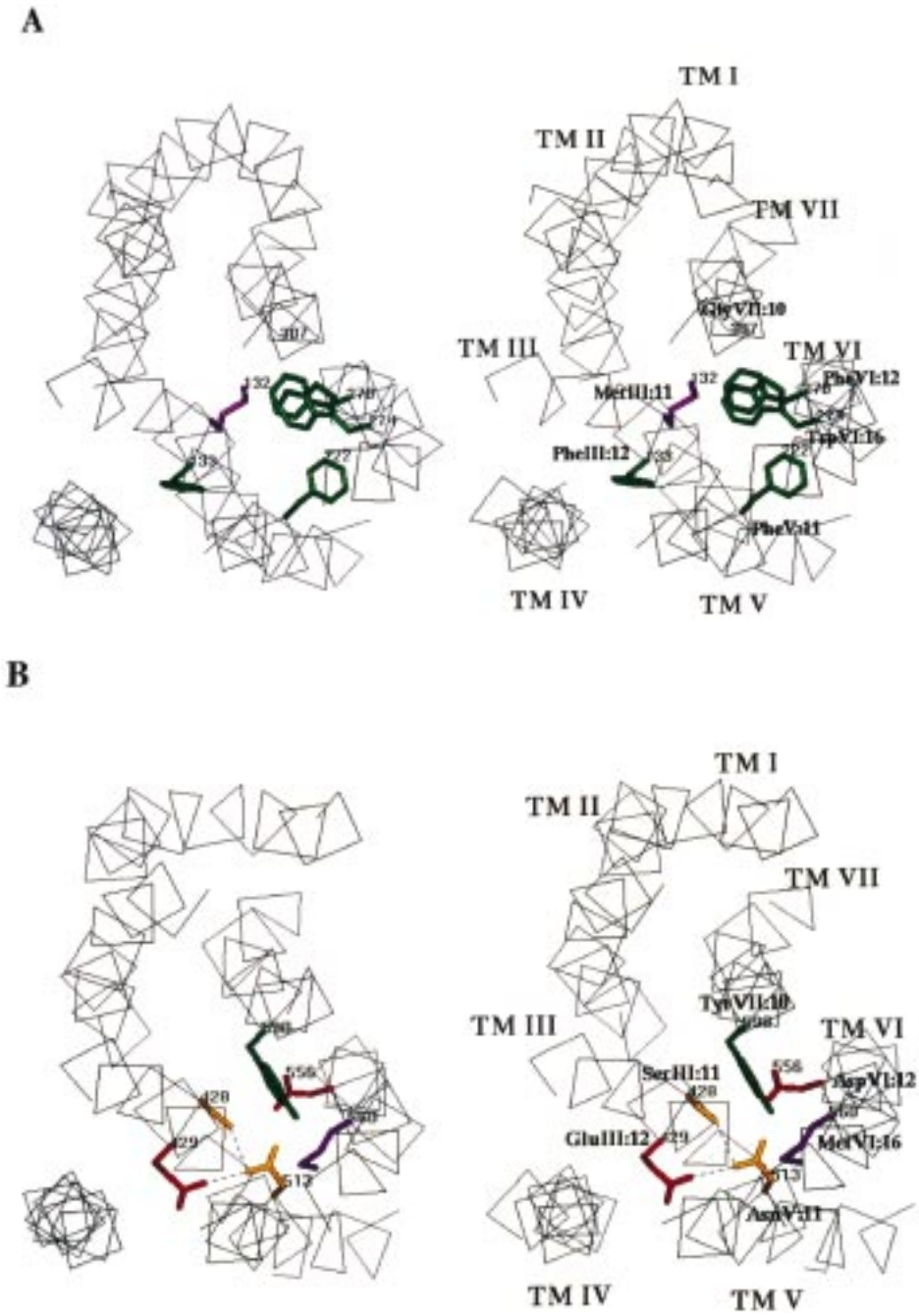

Figure 9. A coordinated replacement of an 'aromatic cluster' present in most GPCRs (A, residues of the δ-opioid receptor are shown) by a polar cluster present only in the glycoprotein hormone receptor subfamily (B, the same residues of lutropin/choriogonadotropin hormone receptor are shown in the same projection). Colors are as in Figure 1. H-bonds are indicated by dashed lines.

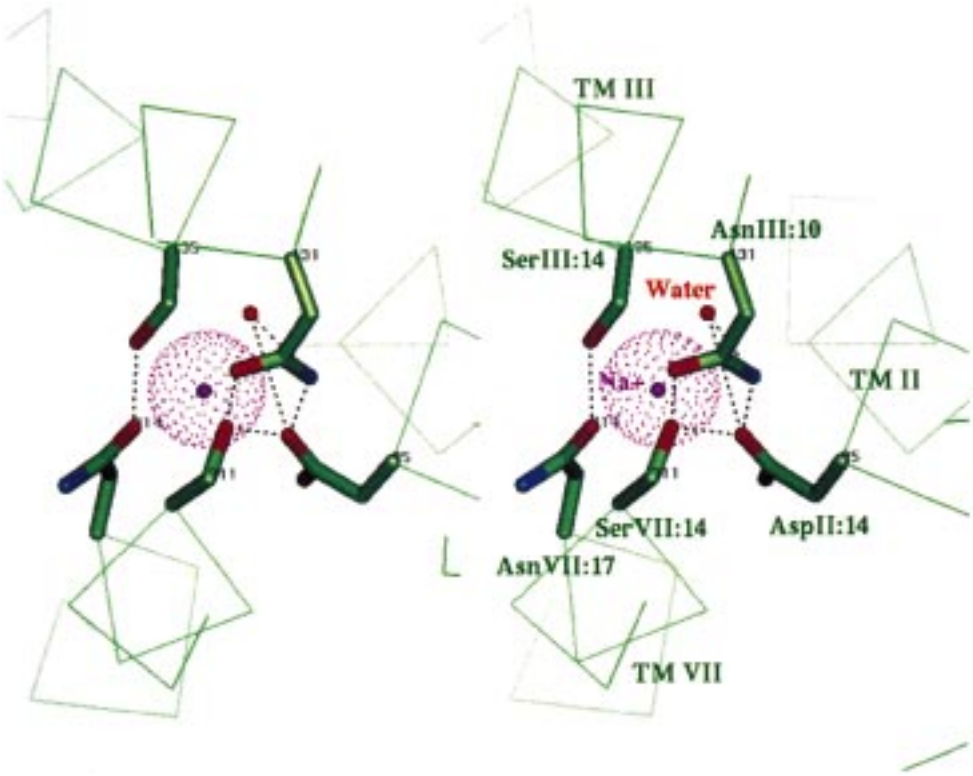

Figure 10. The possible structure of the Na^+-binding center in the δ-opioid receptor. Residues are colored by element, the Na^+ ion is shown as a dotted purple sphere and the tentative water molecule as a dotted red sphere. H-bonds are indicated by dashed lines.

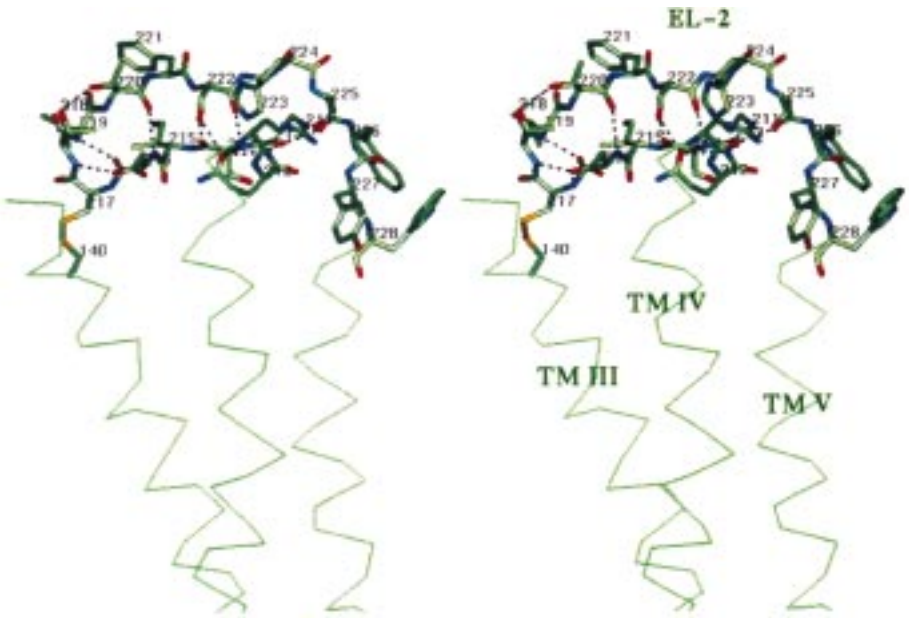

Figure 11. A tentative structure of the second extracellular loop in the μ-opioid receptor, connecting helices IV and V and linked to helix III by a disulfide bond. Residues are colored by element. H-bonds are indicated by dashed lines.

regions, for example, in the N-terminal fragment of μ- and κ-opioid receptors and within EL-1 and EL-3 of purine receptors.

The β-hairpin formed by EL-2 is of special interest. This loop is visible as an elongated, poorly resolved feature in the extracellular part of the 3D EM map of frog rhodopsin [3]. This β-hairpin probably forms an independently stable structure, since antibodies developed against peptide fragments representing EL-2 of several GPCRs recognize the entire receptors and interfere with ligand binding and/or cAMP accumulation [77,87–89]. Moreover, EL-2 may also participate in the activation process, since some GPCRs can be activated by modifications within EL-2 [77] or by antibody binding to the EL-2 region [88,90–93]. In human red opsin, His^{197} and Lys^{200} from EL-2 are involved in spectral tuning of pigments by Cl^- [94]. Thus, this β-hairpin is probably an important structural and functional element that participates in both ligand binding and activation in most GPCRs.

Interestingly, a similar β-hairpin has recently been determined in bacteriorhodopsin by high-resolution electron cryomicroscopy [95]. In bacteriorhodopsin, this β-hairpin occupies the same spatial position as in our rhodopsin model, although it is formed by a different extracellular loop: EL-1 instead of EL-2 as in GPCRs. In bacteriorhodopsin, this β-hairpin also plays a functionally important role as part of the proton-transfer pathway [95].

Coevolution of ligands and their binding pockets

The individual GPCR models were constructed solely from H-bonding constraints, using no information about the receptor ligands. Nevertheless, each model has only one large cavity that can be occupied by ligands (Figures 12–17). In the models of rhodopsins, retinochrome, opioid, melatonin, purine, and cationic amine receptors, the cavities are situated in the same region of the transmembrane domain, between helices II-VII, and are partially covered by extracellular loops.

The bottom of the binding pockets corresponds to the extracellular boundary of the evolutionarily conserved domain of GPCRs (Phe^{212}(V:11), Phe^{261}(VI:12), Cys^{264}(VI:15), Trp^{265}(VI:16), and Ala^{295}(VII:10) in Figure 3). Therefore, there are some clear structural similarities between different GPCRs in this region. The ligand fragments positioned here, i.e. the portion of retinal between the 9-methyl group and the β-ionone ring, Tyr^1 of opioid peptides, the adenine group of ATP, and the catechol moiety of catecholamines, occupy very similar spatial positions (Figure 12) and interact with the same residues. Some of the residues at the bottom of the binding pocket are conserved in most GPCRs, but are replaced in, for example, glycoprotein hormone receptors (Figure 9). Other residues in this region are conserved only in subfamilies of GPCRs and are correlated with ligand structure (for example, in positions III:7, V:7, VI:20, VII:7, and VII:11 shown in Figure 12). The triad of Met I:7, Glu III:3, and Lys VII:11, which interact with the N^+ of the protonated Schiff's base (PSB) in all vertebrate opsins (Figure 7A), is spatially replaced by Trp VII:8, Asp III:7, and Tyr VII:11, respectively, in all cationic amine receptors, where two of these residues (Asp III:7 and Tyr VII:11) form the binding site for the common N^+ of cationic amines (Figures 14–16). This Asp III:7 ... Tyr VII:11 H-bonded pair is also present in opioid receptors, where it, too, forms a binding site for the ligand N^+ (Figure 13).

Retinal-binding pocket The complementarity of the binding cavities to their native and synthetic ligands is evident from their geometrical fit, from the formation of intermolecular H-bonds, and from the clustering of receptor and ligand groups with similar polarities. For example, in bovine rhodopsin, the N^+ of the PSB occupies a polar site that is formed by the carboxylate of Glu^{113}(III:3) (the PSB counterion), the aromatic ring of Phe^{293}(VII:8), the backbone of helix II near Gly^{90}(II:21), the side-chain of Thr^{94}(II:25), and by the δ sulfur of Met^{44}(I:17) (Figure 7A). The polyene chain of 11-*cis* retinal passes through a narrow 'gate' (∼4 Å wide) between helices III and VII, created by residues with small side-chains (Ala^{117}(III:7), Thr^{118}(III:8), Gly^{121}(III:10), Ala^{292}(VII:7), and Ala^{295}(VII:10)). The β-ionone ring occupies a wider (∼7.5 Å) nonpolar cavity surrounded by Leu^{125}(III:15), Phe^{208}(V:7), Phe^{212}(V:11), Phe^{261}(VI:12), Leu^{262}(VI:13), Cys^{264}(VI:15), Trp^{265}(VI:16), and Phe^{294}(VII:9). Thus, the polarities of residues in the binding pocket of rhodopsin match the polarities of contacting retinal groups: the charged PSB of retinal is surrounded by polar side-chains, while the polyene chain and β-ionone ring interact with nonpolar aliphatic and aromatic side-chains. In several invertebrate opsins, polar residues also appear near the β-ionone ring (Ser V:7 and Ser/Asp/Asn VI:23), allowing an H-bond with the OH-group of 3-hydroxy retinal, the native ligand of some invertebrate photopigments [96]. In the crayfish rhodopsin models, Ser^{222}(V:7) forms an H-bond with the 3-OH group of 3-hydroxy-11-*cis* retinal, i.e.

in the inactive receptor state (see Figure 7B), while Asn^{298}(VI:23) can form an H-bond with the 3-OH group of the shifted β-ionone ring in the all-*trans* isomer, i.e. in the photoactivated receptor [16]. The same Ser V:7 and Asn/His VI:23 residues are involved in H-bonds with the catechol ring in adrenergic and dopamine receptor models (Figure 14).

The structures of the binding pockets in various GPCRs are adapted to different ligands by concerted replacements among 20 residues, which transform a nonpolar, narrow, elongated 'cleft' in opsins and retinochrome (Figure 7) to 'L-shaped' binding pockets containing many polar residues in opioid receptors (Figure 13), or to smaller cavities, surrounded by aromatic side-chains, in acetylcholine receptors. However, in cases where the ligand remains the same, the structures of the binding pockets are generally similar, even if the sequence identity of the corresponding GPCRs is low (Figure 7).

An example of remote GPCRs with the same ligand are vertebrate and invertebrate opsins, whose sequence identity is ∼25%. All opsins covalently bind 11-*cis* retinal via a PSB with Lys(VII:11) and convert it to the all-*trans* isomer under illumination, which results in activation of the opsins. The binding pockets of 11-*cis* retinal are very similar in bovine and crayfish rhodopsins, because many key residues in this region are the same: Met I:7, Gly III:11, Trp IV:25, Trp VII:16, Tyr VI:19, Phe VII:9, Ala VII:10, Lys VII:11. However, a few replacements in crayfish rhodopsin shift the β-ionone ring and the adjacent segment of the polyene chain by ∼2.5 Å toward helix IV, while still maintaining a cavity shape appropriate for binding 11-*cis* retinal. This is structurally accomplished by correlated replacements of Phe^{208}(V:7)→Ser^{222} and Phe^{261}(VI:12)→Trp^{287} (Figure 7), which simultaneously increases the volume of a side-chain in one part of the pocket, while decreasing it in another, similar to the 'repacking' of side-chains in remotely related GPCRs (Figure 6). The Ala^{117}(III:7)→Gly^{133} replacement also facilitates the small shift of the polyene chain toward helix III, while the bulky side-chain of Tyr^{309}(VII:7), which appears in place of Ala^{292}, covers the retinal polyene chain from the extracellular side in crayfish rhodopsin (Figure 7B). Tyr^{129}(III:3) in crayfish rhodopsin substitutes for Glu^{133}(III:3), the counterion of the PSB in bovine rhodopsin. The side-chain of Tyr^{129}(III:3) is longer than that of Glu^{133}(III:3) and its OH-group can spatially substitute for the water molecule that H-bonds with the PSB in the bovine rhodopsin model. A cluster of five methionines (Met^{60}(I:7), Met^{102}(II:17), Met^{103}(II:18), Met^{106}(II:21) and Met^{110}(II:25)) surrounds the aromatic side-chain of Tyr^{129}(III:3) in crayfish rhodopsin, in place of Met^{44}(I:7), Met^{86}(II:17), Val^{87}(II:18), Gly^{90}(II:21) and Thr^{94}(II:25) in the vicinity of Glu^{113}(III:3) in bovine rhodopsin.

Squid retinochrome is an example of structural adaptation to a different stereoisomer of the same ligand (Figure 7C). This protein, found in some invertebrates, preferentially binds all-*trans* retinal (instead of the 11-*cis* isomer in rhodopsin) and transforms it to 11-*cis* retinal through all-*trans*→11-*cis* photoisomerization, i.e. it functions in the direction opposite that of rhodopsin [23]. The structure of the retinochrome ligand-binding cavity is very similar to that in bovine rhodopsin (Figures 7A and C), with the similarly located Lys^{271}(VII:11) forming a PSB with all-*trans* retinal. The preferential binding of the all-*trans* isomer instead of 11-*cis* retinal is achieved by coordinated replacements of several residues in the binding pocket. Glu^{113}(III:3), the counterion of the PSB in rhodopsin, is replaced by Met^{93}(III:3) and the only negatively charged residue near Lys^{271}(VII:11) is Asp^{71}(II:21) which probably serves as the counterion for the shifted N^+ group of the PSB in retinochrome. In the E113Q(III:3)/G90D(II:21) rhodopsin double mutant, the corresponding Asp^{90}(II:21) residue can function as an alternative counterion of the PSB [97]. This mutation confers constitutive activity to the receptor, the possible cause of congenital night blindness in patients with G90D(II:21) mutant rhodopsin [97]. In the retinochrome model, this Asp^{71}(II:21) residue forms H-bonds with the ϵ-amino group of Lys^{275}(VII:11) and with His^{268}(VII:4). Compared with bovine rhodopsin, Ala(III:7)→Gly replacement in retinochrome helps to adjust the 13-methyl group of the all-*trans* isomer between helices III and VII, while Ile(V:4)→Phe and Ala(VI:20)→Gly substitutions accommodate the shifted β-ionone ring. The coordinated Thr(III:8)→Phe and Phe(V:7)→Ala replacements move the phenylalanine aromatic ring from V:7 to III:8, i.e. closer to helix III, thus providing space for the 9-methyl group of the all-*trans* isomer. The disappearance of Pro VI:18 decreases the kink in helix VI of retinochrome and shifts this helix closer to helix III. As a result, the β-ionone ring and the 9-methyl group of 11-*cis* retinal in photoactivated retinochrome cannot occupy the same position as in the complex with rhodopsin, due to substantial hindrances with helices III and VI. Therefore, after photoisomerization, 11-*cis*

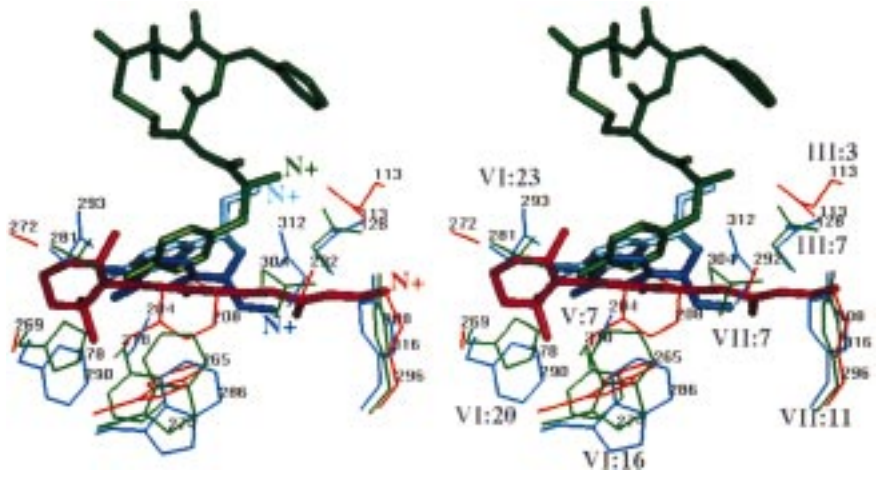

Figure 12. Overlap of several GPCR agonists after superposition of their receptor models: all-*trans* retinal in metarhodopsin II (red), JOM-13 (Tyr-c[D-Cys-Phe-D-Pen]) in the δ-opioid receptor (green), and epinephrine in the β_2-adrenoreceptor (light and dark blue). Epinephrine is shown in two possible orientations, 'upper' (light blue) and 'lower' (dark blue). Several selected residues from the binding pockets are shown by thin lines.

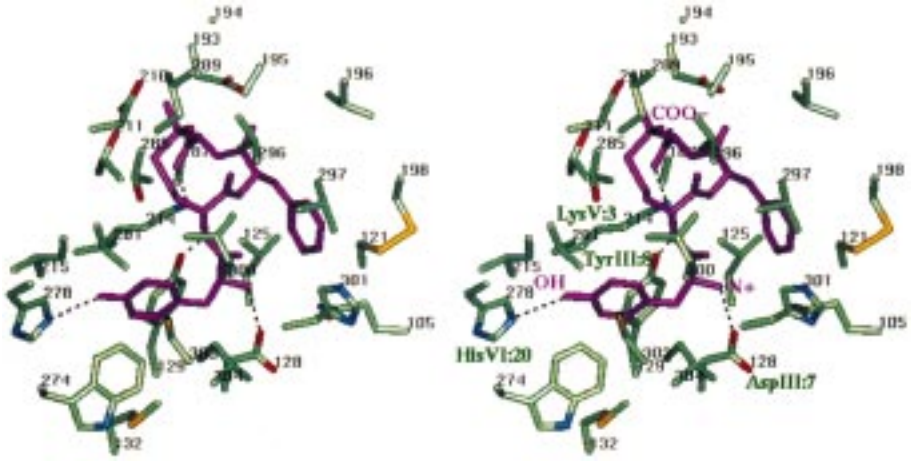

Figure 13. JOM-13 (Tyr-c[D-Cys-Phe-D-Pen]) (magenta) in the binding pocket of the δ-opioid receptor. Residues are colored by element. H-bonds are indicated by dashed lines.

retinal moves toward the extracellular surface and can be released from the binding pocket.

Opioid receptors In opioid receptors (Figure 13), the binding cavity is significantly changed, compared to that in rhodopsin. The binding site of the N^+ group of the retinal PSB between helices II and VII is absent in opioid receptors, with this space now filled by the more bulky residues Tyr I:7, Leu II:21, Tyr II:28, and His/Tyr VII:4. On the other hand, the space between helices III-VII is expanded by Trp(IV:25)→Ala and Tyr(VI:19)→Ile replacements. As a result, the size and shape of the cavity are altered. Furthermore, many residues in the cavity are more polar in the opioid receptors and can form numerous H-bonds with various opioid ligands [17]. The polar residues of opioid receptors in this region are Gln II:24, Asp III:7, Tyr III:8, Asp/Glu V:−1, Thr/Asn V:0, Lys V:3, His VI:20, Thr VI:24, Lys/Glu VI:26, Thr VI:27, Tyr/Trp VII:3, His/Tyr VII:4, and Tyr VII:11. The significance of polar interactions involving Asp III:7, Tyr III:8, His VI:20, and Tyr VII:11 has been demonstrated by site-directed mutagenesis [98–101]. Asp III:7 and His VI:20 residues in the bottom of the binding pocket

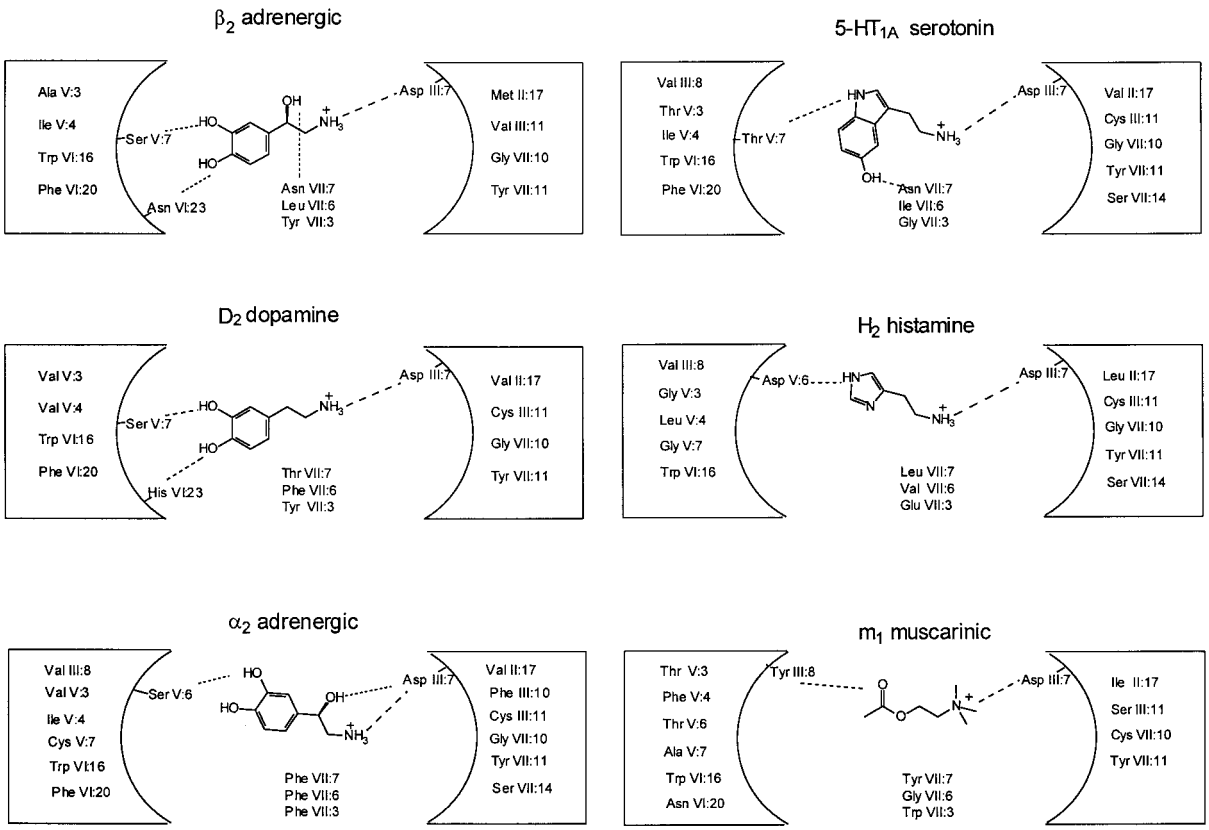

Figure 14. Schematic representation of binding pockets for natural ligands in cationic amine receptors. H-bonds are indicated by dotted lines and electrostatic interactions by dashed lines.

are of special importance, since they serve as two 'attachment points' for the N^+ and OH groups, respectively, of the tyramine moiety common to most opioid ligands (Figure 13, Reference 17). The central, conformationally constrained fragments found in many opioids (e.g. the disulfide-bridged cycles common to several peptide ligands and various ring structures in nonpeptide ligands) are oriented approximately perpendicular to the tyramine and are directed toward the β-hairpin formed by EL- 2 (Figure 13).

Cationic amine receptors The family of cationic amine receptors provides an especially good example for verification of receptor models by ligand docking, since the native ligands for these receptors, i.e. epinephrine, norepinephrine, dopamine, serotonin, histamine, and acetylcholine, have different functional polar groups that are 'mirrored' by corresponding replacements of amino acid residues surrounding the ligands in the binding pockets (Figure 14). In general, the shape of the ligand-binding pocket in cationic amine receptors is similar to that in opioid receptors, since in both subfamilies the space between helices I, II, and VII, which forms part of the retinal-binding site in rhodopsins, is filled by bulky side-chains from positions II:24 (Phe, Trp, Leu), III:3 (Phe, Tyr, Trp), and VII:8 (Trp). However, the cationic amine and opioid receptors have different spatial arrangements of aromatic and polar side-chains, except for the common Asp III:7 ... Tyr VII:11 pair. In cationic amine receptors, aromatic residues are conserved in positions VI:19 (Phe/Tyr), VI:20 (Phe), and VII:3 (Phe/Tyr/Trp) but are never present in position V:7 (Phe in all opioid receptors). The characteristic set of polar residues in the cationic amine subfamily includes Thr III:4, Ser III:11, Thr/Asn III:12, Gln/His/Trp/Arg IV:25, Asp/Ser/Thr V:6, Ser/Thr V:7, Asn/His/Tyr VI:23, Glu/Lys/Asn/His/Tyr VII:3, Asn/Thr/Tyr VII:7, Tyr/Trp VII:11, and Ser VII:14, while positions III:8, V:3, and VI:20 are usually occupied by nonpolar residues.

The ligand-binding cavities of adrenergic, dopamine, serotonin, and histamine receptors (Figures 14–16) are rather similar in size and shape. The aromatic (catechol, indole, or imidazole) rings of their native ligands occupy a binding site formed by aliphatic and aromatic-side chains: Val III:8, Val V:3, Val V:4, Trp VI:16, Phe VI:12, and Phe VI:20, and by polar residues in positions V:6 (Thr, Ser, Asp), V:7 (Thr, Ser), and VI:23 (Asn, His) that can H-bond with polar groups in the rings. Replacement of the ligand aromatic ring by an acetyl group in acetylcholine is correlated with a smaller binding cavity in muscarinic receptors, which results from the appearance of bulky aromatic side-chains of Tyr III:8, Trp IV:18, and Trp VII:3 (Figure 14). The C^{α} and C^{β} atoms of catechol ligands interact with Leu/Phe/Ile/Val VII:6, Asn/Thr/Tyr/Phe/Leu/Val VII:7, and Phe/Tyr VII:3 residues. The common binding site of the amine ligand N^{+} group provides a more polar environment, usually consisting of Asp III:7 (the counterion of N^{+}), the moderately polar Cys/Ser III:11 (Val in β-adrenergic receptors), Gly VII:10, Tyr VII:11, Ser VII:14, and Met/Val/Leu/Ile II:17.

Despite the similarities in the binding pockets, the cationic amine ligands are oriented slightly differently in their receptor models. Two alternate spatial positions of the ligands are possible, one that is common for β-adrenergic and dopamine receptors and another that is characteristic of α-adrenergic, serotonin, and histamine receptors. In the alternate positions, the ligand is shifted in a direction parallel to the membrane plane, similar to the shift of the retinal β-ionone ring in crayfish rhodopsin compared with bovine rhodopsin (Figures 7A and B) or to the shift of the Tyr^{1} of peptide ligands in the μ-opioid receptor compared with the δ-receptor [17]. A comparison of norepinephrine orientations in β_2- and α_2-adrenergic receptors is particularly informative (Figure 15). In the first orientation, as in the β_2-receptor binding site, the ligand catechol ring is positioned between helices V and VI with the *meta*-OH group forming an H-bond with Ser^{204}(V:7) and the *para*-OH group with Asn^{293}(VI:23). The formation of an H-bond between the ligand *meta*-OH group and Ser^{204}(V:7) in the β_2-adrenergic receptor [102], and the involvement of His VI:23 in interactions with *para*-substituents of similarly oriented ligands at the dopamine D_2 receptor [103] have been suggested from mutagenesis data. Another serine from helix V, Ser^{203}(V:6), participates in the H-bond network between helices III, IV, and V (Thr^{118}(III:12)-Ser^{165}(VI:18)-Ser^{203}(V:6)) that may stabilize the transmembrane α-bundle (see Figure 15). These interactions of the Ser^{203}(V:6) residue may explain the incorrect folding observed for S165A and S203A β_2-adrenergic receptor mutants [102]. N^{+} of the ligand is positioned between helices III and VII with additional space available to accommodate different N-substituents (methyl, ethyl, isopropyl groups, etc.). The β-OH group of epinephrine forms an H-bond with Asn^{312}(VII:7) in β_2-adrenergic receptors.

In α_2-adrenergic receptors, the interaction of the catechol ring with Phe^{411}(VII:6) and Phe^{412}(VII:7) shifts the ligand to the second orientation, with the N^{+} and β-OH group ∼2.5 Å closer to helix II and the catechol ring ∼1.5 Å closer to helix IV. As a result, the *meta*-OH group of norepinephrine forms an H-bond with Ser^{200}(V:6) (in place of the corresponding interaction with Ser^{204}(V:7) in β_2-adrenergic receptors) and the ligand aromatic ring approaches Val^{114}(III:8). This is consistent with mutagenesis data obtained from replacement of Ser^{200}(V:6) in α_2- [104] and the corresponding Ser^{188}(V:6) in α_1-adrenergic receptors [105]. The ligand *para*-OH group can H-bond either with the main-chain carbonyl of residue V:3 or with the polar side-chain present in some α-receptors in position V:7. Because of the shift of the ligand N^{+} toward helix II of the α_2-receptor, the β-OH group of norepinephrine forms an H-bond with Asp^{113}(III:7) (instead of Asn^{312}(VII:7), as in β_2-adrenergic receptors). In α-adrenergic receptors, the unoccupied space around the protonated amine decreases and can accommodate only smaller *N*-methyl and *N*-ethyl substituents [106]. In the α_2-receptor model, the α-methyl group of (*S*)(+)-α-methyldopamine occupies a small empty space between Phe^{411}(VII:6) and Gly^{415}(VII:10) that forms the 'third recognition site' [106] in this receptor subtype. This site is absent in the α_1-adrenergic receptor subtype due to Phe VII:6→Leu substitution.

Replacements of residues III:8, V:6, V:7, VI:23, VII:3, and VII:7 in the binding pocket of cationic amine receptors are clearly coordinated with ligand structure (Figure 14). For example, the III:8 position, occupied by nonpolar aliphatic residues in most cationic amine GPCRs, is replaced by Tyr^{106}(III:8) in muscarinic receptors, where the Tyr $O^{\eta}H$ group forms an H-bond with the acetylcholine acetyl group (Figure 14). A similar appearance of Asn VI:23 and His VI:23 residues in β-adrenergic and dopamine receptors, respectively, provides H-bonds with *para*-OH groups of the ligand catechol rings. Asp V:6, present only in histamine H_2 receptors, can form an H-bond

with N^{τ} of histamine, in agreement with mutagenesis data [107], and Glu VII:3 (a position occupied by aromatic residues or Gly in other cationic amine receptors) in the H_2 receptor can interact electrostatically with the ligand imidazole group. Asn VII:7 in β_2-adrenergic and 5-HT_{1A} receptors, which forms an H-bond with the β-OH group of epinephrine and norepinephrine or with the 5-OH group of serotonin, respectively (Figure 14), provides another example. Asn VII:7 has been shown to play an important role in the binding of the β-receptor selective ligands pindolol and propranolol, which possess β-OH groups [108,109]. It has been demonstrated that the human 5-HT_{1B} serotonin receptor, with Thr^{355}(VII:7) in this position, binds pindolol and propranolol poorly, while the T355N(VII:7) 5-HT_{1B} mutant acquires high affinity for these ligands [110]. The absence of a β-hydroxy group in dopamine is correlated with the replacement of Asn VII:7 of β-adrenergic receptors by Thr or Val residues in dopamine receptors. These residues cannot form similar H-bonds with a β-hydroxy substituent.

It should be emphasized that the binding pockets of cationic amine receptors are generally larger than many of their ligands. This leads to the possibility of different arrangements of some ligands in the binding pockets. For example, the β_2-adrenergic agonists norepinephrine and isoproterenol can be inserted in the β_2-receptor model in two alternative orientations, differing primarily in the position of N^+, which can be arranged either below or above Asn^{312}(VII:7) (Figures 12 and 16). In the latter arrangement, N^+ of the ligand is shifted from the bottom of the cavity toward the extracellular surface by 5.2 Å (Figure 16). In the 'lower' arrangement, norepinephrine is situated close to the position of the polyene chain of retinal bound to rhodopsin, while in the 'upper' arrangement it is positioned like the Tyr^1 portion of peptide ligands bound to opioid receptors (Figure 12). The same two alternate positions are also possible for small ligands of other GPCRs, for example for morphine in opioid receptors [17]. In the 'lower' position, the N-isopropyl group of isoproterenol interacts with Met^{82}(II:17), Val^{117}(III:11), Gly^{315}(VII:10), and Tyr^{316}(VII:11), while in the 'upper' position it interacts with Phe^{89}(II:24), Thr^{110}(III:4), His^{173}(IV:25), and Tyr^{308}(VII:3). However, in *both* positions of either norepinephrine or isoproterenol, the N^+ interacts with the same Asp^{113}(III:7) side-chain, the β-hydroxy group forms an H-bond with the same Asn^{312}(VII:7) side-chain, and the catechol ring occupies nearly identical positions and interacts with the same residues (Ile^{201}(V:4), Trp^{286}(VI:16), Phe^{290}(VI:20), and Leu^{311}(VII:6)) and forms H-bonds between its *meta*-OH and *para*-OH substituents and Ser^{204}(V:7) and Asn^{293}(VI:23), respectively (Figure 16).

All native cationic amine ligands described above (Figures 14 and 15) were docked in the lower position, although in most cases the alternative upper positions are also possible. Most larger, synthetic ligands can be inserted in the binding pockets in only one of these positions. For example, the β-antagonist carazolol can occupy only the lower position in the binding pocket because of hindrances between its ring system and residues from helix V in the upper ligand orientation. In contrast, the β_2-affinity label [^{125}I]iodoazidobenzylpindolol, which binds irreversibly to the β_2-adrenergic receptor [111], can be arranged only in the upper position. In the β_2-receptor model, the azido group of this label can be cross-linked to the $N^{\epsilon 1}$ groups of either Trp^{330}(VII:8) or Trp^{109}(III:3), depending on the rotamer of the phenyl ring of the label (the corresponding N...N distances are 3.0 and 3.5 Å, respectively). This agrees with experimental data that implicate Trp^{330}(VII:8) and another unidentified residue between helices III and V as two sites of covalent labeling by the β_2-affinity reagent [111]. Similarly, some high-affinity α-receptor agonists with bulky phenyl-containing N-substituents [108] can be accommodated in the binding pocket only in the upper position.

Comparison of GPCR models with experimental data

The individual GPCR models are consistent with experimental data that were not considered in the calculations and which can therefore be used for verification. The model of rhodopsin, for example, is in agreement with a vast collection of published biophysical data, such as the arrangement of α-helices in the low-resolution 3D EM maps; mapping of water- and lipid-accessible rhodopsin residues by chemical probes; identification of residues surrounding retinal by site-directed mutagenesis and cross-linking; orientations of all-*trans* and 11-*cis* retinal relative to the membrane plane and the distances from the ligand to the intra- and extracellular surfaces, determined by linear dichroism and fluorescence quenching; reconstitution studies of opsin with synthetic retinal analogues; the conformation and environment of the PSB formed between Lys^{296}(VII:11) and 11-*cis* reti-

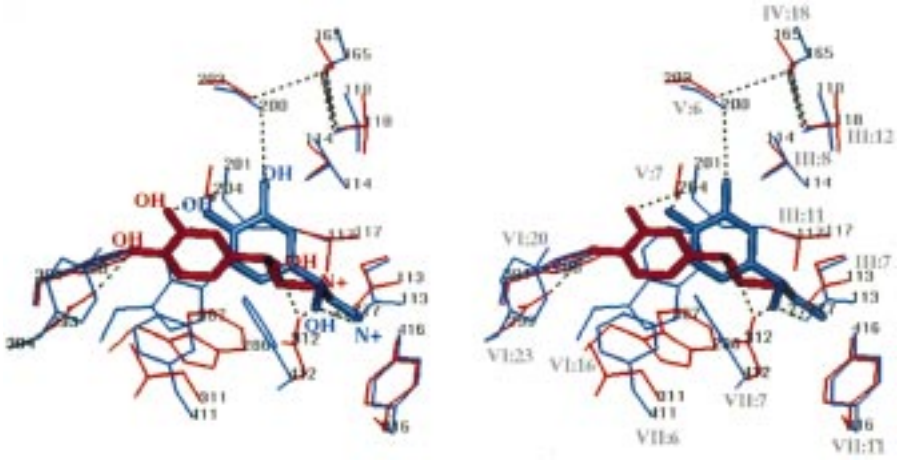

Figure 15. Different positions of norepinephrine in the binding pockets of β_2 (red) and α_2 (blue) adrenergic receptors. Selected residues from the binding pockets are shown by thin lines and H-bonds are indicated by dashed lines.

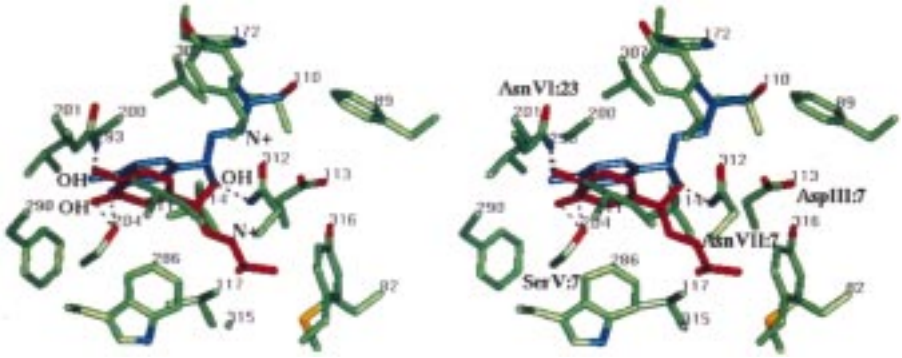

Figure 16. 'Upper' (blue) and 'lower' (red) positions of norepinephrine in the β_2-adrenoreceptor binding pocket. Residues are colored by element. H-bonds are indicated by dashed lines.

nal, studied by Raman, FTIR, and ^{13}C solid-state NMR spectroscopies; compensatory replacements of the Glu^{113}(III:3) by Asp^{90}(II:21) or Asp^{117}(III:7) residues, and many others [16]. The possibility of H-bonds between pairs of polar residues (II:14 and VII:17, II:28 and VII:3, and III:7 and VII:4) in the model is also in agreement with constraints experimentally derived from site-directed mutagenesis, such as the proximity of Asn^{87}(II:14) and Asn^{318}(VII:17) in the gonadotropin-releasing hormone receptor [66], Asp^{120}(II:14) and Asn^{396}(VII:17) in the 5-HT_{2A} receptor [65], Asp^{397}(II:28) and Lys^{583}(VII:3) in the lutropin/choriogonadotropin hormone receptor [112], and Asp^{125}(III:7) and Lys^{331}(VII:4) in α_{1B}-adrenergic receptors [113]. The model is also consistent with the formation of artificial Zn^{2+}-binding sites in the NK-1 [114] and κ-opioid receptors [115] by histidines present in positions V:−1, V:3, and VI:27 of mutant receptors [16].

A comparison of our rhodopsin model and a recently published EM-based C^{α} atom template [15] shows that they are rather similar (Figure 17). The observed 3.3 Å rmsd (for 169 common C^{α} atoms) originates mostly from small outward shifts of TMH II and the C-terminus of TMH III, and from ∼3 Å shifts of TMH V and TMH VI in the direction perpendicular to the membrane plane in the EM-based model relative to ours. This can be partially attributed to some errors in the EM-based model [15]. Since the individual residues are not visible in the EM maps (the resolution is 7.5 Å in the membrane plane and 16.5 Å in the perpendicular direction), the TMHs were approximately positioned by translating and rotating them to orient their most conserved residues within the α-bundle and to align the most hydrophobic portions of the helices in the normal to the membrane. As a result, and as was discussed by Baldwin et al. [15], this model contradicts some experimental data, such as

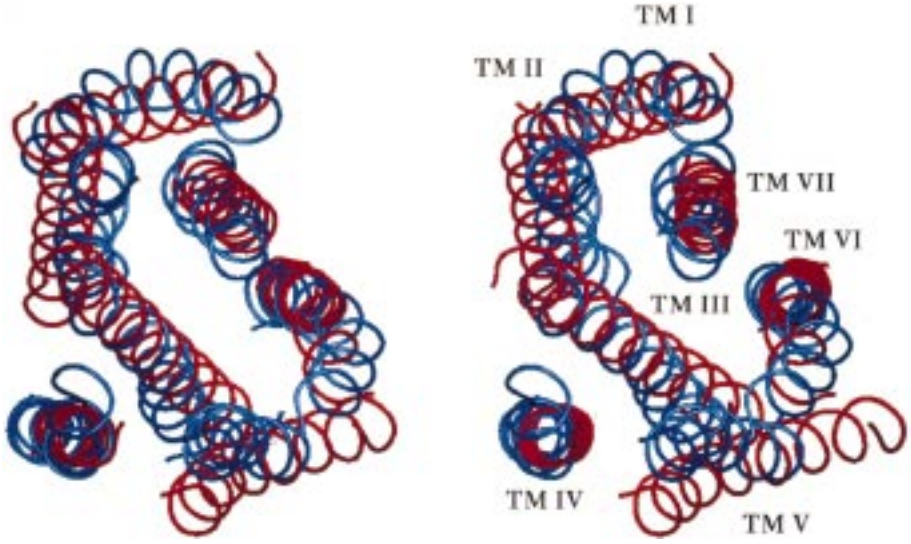

Figure 17. Superposition of the bovine rhodopsin model calculated with H-bond constraints (PDB file: 1bok, blue) and the C^{α} atom template obtained by fitting ideal helices to the 7.5 Å resolution EM map of frog rhodopsin (Reference 15, red). The C^{α} atoms of common residues in the models (segments 38–64, 71–94, 111–141, 151–175, 204–223, 247–274, and 288–310) were superimposed (bovine rhodopsin sequence numbering).

the formation of a Zn^{2+}-binding cluster by histidines incorporated into the extracellular ends of TMH V and TMH VI [114,115] and site-directed mutagenesis results that reveal the spatial proximity of residues of TMH III and TMH V that participate in the binding of catecholamines [65,66,102,120–122]; the proximity of conserved Asp and Asn residues of TMH II and TMH VII, respectively; and the proximity of Gly^{121} (TMH III) and Phe^{261} (TMH VI) in bovine rhodopsin [123,124]. All these data are satisfied in our model.

On the other hand, some recent experimental data suggest that our model may be flawed on the intracellular side of the transmembrane α-bundle: TMH V is probably longer and more tilted than in our model and TMH VI may be shifted in the vertical direction toward the intracellular surface to bring together histidine residues incorporated into the ends of TMH III and TMH VI that can form a Zn^{2+}-binding cluster in rhodopsin mutants [117]. We are presently investigating these alternatives.

As noted in the preceding sections, the vast majority of available mutagenesis data is in excellent agreement with our models of cationic amine receptors. The importance of aromatic residues Phe VI:20 in β-adrenergic and 5-HT_{2A} receptors and residues Tyr(III:8), Tyr(VI:20), Tyr(VII:7), Tyr(VII:11) in muscarinic receptors has been shown by Strader et al. [125], Choudhary et al. [126,127], and Wess et al. [122, 128]. The 'key' role of Asp(III:7) in the binding of amines has been demonstrated by point mutations of β_2-adrenergic receptors [102,120,121], α_{1B}-adrenergic receptors [113], α_{2A}-adrenergic receptors [104], m_1 muscarinic receptors [129], histamine receptors [130], dopamine receptors [131,132], and 5-HT_{1A} and 5-HT_2 receptors [133,134]. It has also been demonstrated that many polar residues which form H-bonds with various cationic amine ligands in our models are important for ligand binding: Ser/Thr V:6, Ser/Thr/Asp V:7, Ser V:10 [102,104,105,107,122,128,135,136], Ser III:11 [137], Tyr III:8, Tyr VI:19 [122,128], Asn VI:20 [138], His VI:23 [103], Asn/Thr/Tyr VII:7 [108–110,122, 128], Tyr VII:11 [122,128], and Ser VII:14 [54]. The models are also consistent with the accessibilities of residues from helices III, V, and VII to chemical modification by water-soluble probes, which were determined by cysteine-scanning mutagenesis of the dopamine D_2 receptor [89,139,140]. In the D_2 receptor model, residues III:1, III:3, III:4, III:7, III:8, III:11, V:3, V:4, V:6, V:7, V:8, V:11, VII:2, VII:3, VII:4, VII:6, VII:7, VII:8, VII:10, and VII:11 are accessible to water because they are situated in the binding pocket, consistent with the labeling data. A number of other polar residues of dopamine receptors (III:14, III:18, III:22, V:22, VII:13, VII:17, and VII:21) are situated within the α-bundle in the model, where they form extensive hydrophilic clusters and can be partially hydrated. It has been shown that all these polar

residues as well as several adjacent residues (III:15, III:18, V:10, V:13, V:14, and VII:18) and a few residues located close to the helix ends (III:2, V:2, V:5, V:9, and VII:5) are also accessible for chemical modification by hydrophilic probes [89,139,140].

In several cases, analysis of our models suggests some alternative interpretations of previously published experimental data. For example, in the β_2-adrenergic receptor model the *meta*-hydroxy group of the ligand's catechol ring forms an H-bond with Ser^{204}(V:7), as has previously been suggested from decreased binding of isopreterenol analogs to the S204A (V:7) mutant of the β_2-adrenergic receptor [102,125]. However, the *para*-hydroxy group of the catechol ring forms an H-bond with Asn^{293}(VI:23), instead of with Ser^{207}(V:10), as has been proposed based upon mutagenesis data [102]. The uncertain role of serine residues of helix V in H-bonding with adrenergic ligands has recently been debated in the literature [71,141,142]. In our adrenergic receptor models, Ser^{207}(V:10), which is conserved in the amine receptor subfamily, does not interact directly with ligands but rather participates in an H-bond network between helices III, IV, and V, formed by the side-chains of Glu^{122}(III:16), Ser^{161}(IV:14), and Ser^{207}(V:10), all of which are conserved in β-receptors. Thus, replacements of Ser^{207}(V:10) would be expected to primarily affect activation of the receptor. In fact, this is consistent with the data of Strader et al. [102], which show that the binding of an isoproterenol analog with only a *para*-hydroxy substituent to the S207A mutant was virtually unaffected but that activation of the mutant receptor was profoundly diminished. Similar results indicating an important role of Ser(V:10) in receptor activation have been obtained more recently for several other cationic amine receptors [104,105,135,136].

Conclusions

We have described, above, some of the general features of the 7-α-helical domains of 26 different GPCRs and two related proteins, retinochrome and the Duffy erythrocyte antigen, calculated using a distance geometry approach. The computational procedure represents a 'large-scale' refinement of an approximate model of the transmembrane 7-α-bundle constructed from electron microscopy and other experimental data. This refinement of the α-bundle was not based on energy minimization, since the existing theoretical approaches do not allow calculation of the appropriate energy. Instead, structural constraints encoded in the multiple sequence alignments of GPCRs, i.e. the experimental data provided by natural mutagenesis and natural selection during many millions of years of evolution, were used.

The rhodopsin-like GPCR family includes hundreds of proteins with amino acid sequence identities in the range of 20–99%. Comparisons of GPCRs with low sequence identity are especially informative, since such receptors feature alternative versions of side-chain packing which must be accommodated within the same, common 3D structure. Site-directed mutagenesis studies of many proteins indicate that replacements of inner, tightly packed residues are usually destructive, and that the design of stable and functional mutants with an alternatively repacked 'core' is a challenging problem, since this requires correlated, compensatory replacements of several interacting residues. The GPCR family, however, provides a multitude of such correlated replacements in the core created by natural selection, which can be transformed into structural constraints.

The correlated replacement of core residues during protein evolution is accomplished such that the interacting side-chains of the transmembrane helices maintain matching polarities, provide geometrically close packing, and, if polar, form interhelical H-bonds. Only these H-bonds, collected from many different GPCRs, were used for calculations of the α-bundle, since they give the most unequivocal and restrictive distance constraints. Nevertheless, the analysis of the 28 calculated structures reveals not only 'saturation of H-bond potential' for buried polar side-chains, but also close packing of nonpolar side-chains, the formation of extensive aromatic and sulfur–aromatic clusters (aromatic residues usually separate polar and aliphatic regions, creating polarity gradients), an anisotropic distribution of lipid-facing side-chains whose polarities match the nonpolar tails and polar head groups of the lipids, the formation of a regulatory Na^+-binding site, and the existence, in many GPCRs, of interhelical disulfide bonds. The models are further characterized by a single, common ligand-binding region that, for 17 GPCRs examined, is complementary in shape and polarity to the corresponding native and synthetic ligands. Moreover, the models of bovine rhodopsin, opioid, and cationic amine receptors are consistent with a vast sample of published experimental data.

Acknowledgements

This work was supported by grants DA03910, DA09989, and DA00118 from the National Institutes of Health and by an Upjohn Research Award from the College of Pharmacy of the University of Michigan. I.D.P. was supported by NIDA training grant DA07268.

References

1. Watson, S. and Arkinstall, S., The G-Protein Linked Receptor Facts Book, Academic Press, San Diego, CA, 1994, pp. 1–294.
2. Unger, V.M. and Schertler, G.F.X., Biophys. J., 68 (1995) 1776.
3. Unger, V.M., Hargrave, P.A., Baldwin, J.M. and Schertler, G.F.X., Nature, 389 (1997) 203.
4. Davies, A., Schertler, G.F.X., Gowen, B.E. and Saibil, H.R., J. Struct. Biol., 117 (1996) 36.
5. Baldwin, J.M., EMBO J., 12 (1993) 1693.
6. Chothia, C. and Lesk, A.M., EMBO J., 5 (1986) 823.
7. Donnelly, D., Overington, J.P., Ruffle, S.V., Nugent, J.H.A. and Blundell, T.L., Protein Sci., 2 (1993) 55.
8. Taylor, W.R., Jones, D.T. and Green, N.M., Proteins Struct. Funct. Genet., 18 (1994) 281.
9. Donnelly, D., Findlay, J.B.C. and Blundell, T.L., Receptors Channels, 2 (1994) 61.
10. Lin, S.W., Imamoto, Y., Fukada, Y., Shichida, Y., Yoshizawa, T. and Mathies, R.A., Biochemistry, 33 (1994) 2151.
11. Kim, J.J., Wess, A.M., van Rhee, A.M., Schoneberg, T. and Jacobson, K.A., J. Biol. Chem., 270 (1995) 13987.
12. Herzyk, P. and Hubbard, R.E., Biophys. J., 69 (1995) 2419.
13. Donnelly, D. and Findlay, J.B.C., Curr. Opin. Struct. Biol., 4 (1994) 582.
14. Ballesteros, J.A. and Weinstein, H., Methods Neurosci., 25 (1995) 366.
15. Baldwin, J.M., Schertler, G.F.X. and Unger, V.M., J. Mol. Biol., 272 (1997) 144.
16. Pogozheva, I.D., Lomize, A.L. and Mosberg, H.I., Biophys. J., 70 (1997) 1963.
17. Pogozheva, I.D., Lomize, A.L. and Mosberg, H.I., Biophys. J., 75 (1998) 612.
18. McDonald, I.K. and Thornton, J.M., J. Mol. Biol., 238 (1994) 777.
19. Güntert, P., Brawn, W. and Wüthrich, K., J. Mol. Biol., 217 (1991) 517.
20. Hara-Nishimura, I., Kondo, M., Nishimura, M., Hara, R. and Hara, T., FEBS Lett., 335 (1993) 94.
21. Horuk, R., Trends Pharmacol. Sci., 151 (1994) 159.
22. Ptitsyn, O.B. and Finkelstein, A.V., Q. Rev. Biophys., 13 (1980) 339.
23. Dill, K.A., Biochemistry, 29 (1990) 7133.
24. Scholtz, J.M., Marqusee, S., Baldwin, R.L., York, E.J., Stewart, J.M., Santoro, M. and Bolen, D.W., Proc. Natl. Acad. Sci. USA, 88 (1991) 2854.
25. Scholtz, J.M., Qian, H., Robbins, V.H. and Baldwin, R.L., Biochemistry, 32 (1993) 9668.
26. Huyghues-Despointes, B., Klinger, T.M. and Baldwin, R.L., Biochemistry, 34 (1995) 13267.
27. Lamba, O.P., Borchman, D. and O'Brien, P.J., Biochemistry, 33 (1994) 1704.
28. Rees, D.C., DeAntonio, L. and Eisenberg, D., Science, 245 (1989) 510.
29. Deisenhofer, J. and Michel, H., Annu. Rev. Cell Biol., 7 (1991) 1.
30. Henderson, R., Baldwin, J.M., Ceska, T.A., Zemlin, F., Beckmann, E. and Downing, K.H., J. Mol. Biol., 213 (1990) 899.
31. Grigorieff, N., Ceska, T.A., Downing, K.H., Baldwin, J.M. and Henderson, R., J. Mol. Biol., 259 (1996) 393.
32. Tsukihara, T., Aoyama, H., Yamashita, E., Tomikazi, T., Yamaguchi, H., Shinzawa-Itoh, K., Nakashima, R., Yaono, R. and Yoshikawa, S., Science, 272 (1996) 1136.
33. Doyle, D.A., Cabral, J.M., Pfuetzner, R.A., Kuo, A., Gulbis, J.M., Cohen, S.L., Chait, B.T. and MacKinnon, R., Science, 280 (1998) 69.
34. Xia, D., Yu, C.-A., Kim, H., Xia, J.-Z., Kachurin, A.M., Zhang, L., Yu, L. and Deisenhofer, J., Science, 277 (1997) 60.
35. Schultz, G.E., In Pullman et al. (Eds.) Membrane Proteins: Structures, Interactions and Models, Kluwer Academic Publishers, Dordrecht, 1992, pp. 403–412.
36. Lomize, A.L., Orekhov, V.Yu. and Arseniev, A.S., Bioorg. Khim., 18 (1992) 182.
37. White, S.H. and Wimley, W.C., Curr. Opin. Struct. Biol., 4 (1994) 79.
38. Wimley, W.C. and White, S.H., Biochemistry, 32 (1993) 6307.
39. Bystrov, V.F., Arseniev, A.S., Barsukov, I.L., Lomize, A.L., Abdulaeva, G.V., Sobol, A.G., Maslennikov, I.V. and Golovanov, A.P., In Jardetzky, O. (Ed.) Protein Structure and Engineering, NATO ASI Series A, Vol. 183, 1989, pp. 111–138.
40. Richards, F.M. and Lim, W.A., Q. Rev. Biophys., 26 (1994) 423.
41. Matsumura, M. and Matthews, B.W., Methods Enzymol., 202 (1991) 336.
42. Clarke, J., Henrick, K. and Fersht, A.R., J. Mol. Biol., 253 (1995) 493.
43. Christianson, D.W., Adv. Protein Chem., 42 (1991) 281.
44. Rao, V.R., Cohen, G.B. and Oprian, D.D., Nature, 367 (1994) 639.
45. Soppa, J., FEBS Lett., 342 (1994) 7.
46. Murzin, A.G., EMBO J., 12 (1993) 861.
47. Murzin, A.G., Curr. Opin. Struct. Biol., 6 (1996) 386.
48. Altschuh, D., Vernet, T., Berti, P., Moras, D. and Nagai, K., Protein Eng., 2 (1988) 193.
49. Neher, E., Proc. Natl. Acad. Sci. USA, 91 (1994) 98.
50. Gobel, U., Sander, C., Schneider, R. and Valencia, A., Proteins Struct. Funct. Genet., 18 (1994) 309.
51. Shindyalov, I.N., Kolchanov, N.A. and Sander, C., Protein Eng., 3 (1994) 349.
52. Taylor, W.R. and Hartrick, K., Protein Eng., 7 (1994) 341.
53. Nakayama, T.A. and Khorana, H.G., J. Biol. Chem., 266 (1991) 4269.
54. Chanda, P.K., Minchin, M.C., Davis, A.R., Greenberg, L., Reilly, Y., McGregor, W.H., Bhat, R., Lubeck, M.D., Mizutani, S. and Hung, P.P., Mol. Pharmacol., 43 (1993) 516.
55. Ceresa, B.P. and Limbird, L.E., J. Biol. Chem., 269 (1994) 29557.
56. Laue, L., Chan, W.Y., Hsueh, A.J., Kudo, M., Hsu, S.Y., Wu, S.M., Blomberg, L. and Cutler Jr., G.B., Proc. Natl. Acad. Sci. USA, 92 (1995) 1906.

57. Monnot, C., Bihoreau, C., Conchon, S., Curnow, K.M., Corvol, P. and Clauser, E., J. Biol. Chem., 271 (1996) 1507.
58. Fernandez, L.M. and Puett, D., Biochemistry, 35 (1996) 3986.
59. Sakmar, T.P., Franke, R.R. and Khorana, H.G., Proc. Natl. Acad. Sci. USA, 86 (1989) 8309.
60. Cohen, G.B., Yang, T., Robinson, P.R. and Oprian, D.D., Biochemistry, 32 (1993) 6111.
61. Fahmy, K., Jäger, F., Beck, M., Zvyaga, T.A., Sakmar, T.P. and Seibert, F., Proc. Natl. Acad. Sci. USA, 90 (1993) 10206.
62. Hunyady, L., Bor, M., Balla, T. and Catt, K.J., J. Biol. Chem., 270 (1995) 9702.
63. Rath, P., DeCaluwé, L.L.J., Bovee-Geurts, P.H.M., DeGrip, W. J. and Rothschild, K.J., Biochemistry, 32 (1993) 10277.
64. Hwa, J., Gaivin, R., Porter, J.E. and Perez, D.M., Biochemistry, 36 (1997) 633.
65. Sealfon, S.C.L., Chi, B.J., Ebersole, B.J., Rodic, V., Zhang, D., Ballesteros, J.A. and Weinstein, H., J. Biol. Chem., 270 (1995) 16683.
66. Zhou, W., Flanagan, C., Ballesteros, J.A., Konvicka, K., Davidson, J.S., Weinstein, H., Millar, R.P. and Sealfon, S.C., Mol. Pharmacol., 45 (1994) 165.
67. Horstman, D.A., Brandon, S., Wilson, A.L., Guyer, C.A., Cragoe Jr., E.J. and Limbird, L.E., J. Biol. Chem., 265 (1990) 21590.
68. Quintana, J., Wang, H. and Ascoli, M., Mol. Endocrinol., 7 (1993) 767.
69. Kong, H., Raynor, K., Yasuda, K., Bell, G.I. and Reisine, T., Mol. Pharmacol., 44 (1993) 380.
70. Kong, H., Raynor, K., Yasuda, K., Moe, S.T., Portoghese, P.S., Bell, G.I. and Reisine, T., J. Biol. Chem., 268 (1993) 23055.
71. Schwartz, T.W. and Rosenkilde, M.M., Trends Pharmacol. Sci., 17 (1996) 347.
72. Metzger, T.G., Paterline, M.G., Portoghese, P.S. and Ferguson, D.M., Neurochem. Res., 21 (1996) 1287.
73. Doi, M., Ishida, T. and Inoue, M., Chem. Pharm. Bull., 38 (1990) 1815.
74. Lerner, D.J., Chen, M., Tram, T. and Coughlin, S.R., J. Biol. Chem., 271 (1996) 13943.
75. Olah, M.E., Jacobson, K.A. and Stiles, G.L., J. Biol. Chem., 269 (1994) 24692.
76. Walker, P., Munoz, M., Martinez, R. and Peitsch, M.C., J. Biol. Chem., 269 (1994) 2863.
77. Nanevicz, T., Wang, L., Chen, M., Ishii, M. and Coughlin, S.R., J. Biol. Chem., 271 (1996) 702.
78. Noda, K., Saad, Y., Graham, R.M. and Karnik, S.S., J. Biol. Chem., 269 (1994) 6743.
79. Couture, L., Remy, J.-J., Rabesona, H., Troalen, F., Pajot-Augy, E., Bozon, V., Haertle, T., Bidart, J.-M. and Salesse, R., Eur. J. Biochem., 241 (1996) 627.
80. Fitzpatrick, V.D. and Vandlen, R.L., J. Biol. Chem., 269 (1994) 24621.
81. Roglic, A., Prossniz, E.R., Cavanagh, S.L., Pan, Z., Zou, A. and Ye, R.D., Biochim. Biophys. Acta, 1305 (1996) 39.
82. Sibanda, B.L. and Thornton, J.M., Methods Enzymol., 202 (1991) 59.
83. DeAlba, E., Jiménez, M.A., Rico, M. and Nieto, J., Folding Design, 1 (1996) 133.
84. Richardson, J.S. and Richardson, D.C., In Fasman, G.D. (Ed.) Prediction of Protein Structure and the Principles of Protein Conformation, Plenum, New York, NY, 1989, pp. 2–97.
85. Hebert, C.A., Chuntharapai, A., Smith, M., Colby, T., Kim, J. and Horuk, P., J. Biol. Chem., 268 (1993) 18549.
86. Schwartz, T.W., Gether, U., Schambye, H.T. and Hjorth, S.A., Curr. Pharmacol. Design, 1 (1995) 325.
87. Abd Alla, S., Quitterer, U., Grigoriev, S., Maidhof, A., Haasemann, M., Jarnagin, K. and Müller-Ester, W., J. Biol. Chem., 271 (1996) 1748.
88. Verdot, L., Bertin, B., Guilloteau, D., Strosberg, A.D. and Hoebeke, J., J. Neurochem., 65 (1995) 319.
89. Fu, M.L.X., Schulze, W., Wallukat, G., Hjalmarson, A. and Hoebeke, J., Clin. Immunol. Immunopathol., 78 (1996) 203.
90. Endo, T., Ohmori, M., Ikeda, M. and Onaya, T., Biochem. Biophys. Res. Commun., 181 (1991) 1035.
91. Kaneshige, M., Haraguchi, K., Endo, T., Anzai, E. and Onaya, T., Horm. Metab. Res., 27 (1995) 267.
92. Fu, M.L.-X., Schulze, W., Wallukat, G., Hjalmarson, A. and Hoebeke, J., J. Mol. Cell. Cardiol., 27 (1995) 427.
93. Zhao, R., Wang, W., Wu, B., Hoebeke, J., Hjalmarson, A. and Fu, M.L.X., Mol. Cell. Biochem., 163/164 (1996) 185.
94. Wang, Z., Asenjo, A.B. and Oprian, D.D., Biochemistry, 32 (1993) 2125.
95. Kimura, Y., Vassylyev, D., Miyazawa, A., Kidera, A., Matsushima, M., Mitsuoka, K., Murata, K., Hirai, T. and Fujiyoshi, Y., Nature, 389 (1997) 206.
96. Vogt, K., Photochem. Photobiol. (Suppl.) (1987) 273.
97. Rao, V.R. and Oprian, D.D., Annu. Rev. Biophys. Biomol. Struct., 25 (1996) 287.
98. Befort, K., Tabbara, L.P., Bausch, S., Chavkin, C., Evans, C. and Kieffer, B.L., Mol. Pharmacol., 49 (1996) 216.
99. Befort, K., Tabbara, L.P., Kling, D., Maigret, B. and Kieffer, B.L., J. Biol. Chem., 271 (1996) 10161.
100. Surratt, C.K., Johnson, P.S., Moriwaki, A., Seidleck, B.K., Blaschak, C.J., Wang, J.B. and Uhl, G.R., J. Biol. Chem., 269 (1994) 20548.
101. Mansour, A., Taylor, L.P., Fine, J.L., Thompson, R.C., Hoversten, M.T., Mosberg, H.I., Watson, S.J. and Akil, H., J. Neurochem., 68 (1997) 344.
102. Strader, C.D., Candelore, M.R., Hill, W.S., Sigal, I.S. and Dixon, R.A.F., J. Biol. Chem., 264 (1989) 13572.
103. Woodward, R., Daniell, S.J., Strange, P.G. and Naylor, H., J. Neurochem., 62 (1994) 1664.
104. Wang, C.-D., Buck, M.A. and Fraser, C.M., Mol. Pharmacol., 40 (1991) 168.
105. Hwa, J. and Perez, D.M., J. Biol. Chem., 271 (1996) 6322.
106. Timmermans, P.B.M.W.M., Chiu, A.T. and Thoolen, M.J.M.C., In Hansch, G., Sammes, P.G. and Taylor, J.B. (Eds.) Comprehensive Medicinal Chemistry, Vol. 3, Pergamon, Oxford, 1990, pp. 133–185.
107. Gantz, I., DelValle, J., Wang, L., Tashiro, T., Munzert, G., Guo, Y., Konda, Y. and Yamada, T., J. Biol. Chem., 267 (1992) 20840.
108. Suryanarayana, S., Daunt, D.A., Von Zastrow, M. and Kobilka, B.K., J. Biol. Chem., 266 (1991) 15488.
109. Guan, X.-M., Peroutka, S. and Kobilka, B.K., Mol. Pharmacol., 41 (1992) 695.
110. Parker, E.M., Grisel, D.A., Iben, L.G. and Shapiro, R.A., J. Neurochem., 60 (1993) 380.
111. Wong, S.K.-F., Slaughter, C., Ruoho, A. and Ross, E.M., J. Biol. Chem., 263 (1988) 7925.
112. Fernandez, L.M. and Puett, D., J. Biol. Chem., 271 (1996) 925.
113. Porter, J.E., Hwa, J. and Perez, D.M., J. Biol. Chem., 45 (1996) 28318.

114. Elling, C.E., Nielsen, S.M. and Schwartz, T.W., Nature, 374 (1995) 74.
115. Thirstrup, K., Elling, C.E., Hjorth, S.A. and Schwartz, T.W., J. Biol. Chem., 271 (1996) 7875.
116. Farrens, D.L., Altenbach, C., Yang, K., Hubbell, W.L. and Khorana, H.G., Science, 274 (1996) 768.
117. Sheikh, S., Zviaga, T.A., Lichtarge, O., Sakmar, T.P. and Bourne, H.R., Nature, 383 (1996) 347.
118. Oliviera, L., Paiva, C.M. and Vriend, G., J. Comput.-Aided Mol. Design, 7 (1993) 649.
119. Yu, H., Kono, M., McKee, T.D. and Oprian, D.D., Biochemistry, 34 (1995) 14963.
120. Strader, C.D., Sigal, I.S., Register, R.B., Candelore, M.R., Rands, E. and Dixon, R.A.F., Proc. Natl. Acad. Sci. USA, 84 (1987) 4384.
121. Strader, C.D., Sigal, I.S., Candelore, M.R., Rands, E., Hill, W.S. and Dixon, R.A.F., J. Biol. Chem., 263 (1988) 10267.
122. Wess, J., Gdula, D. and Brann, M.R., EMBO J., 10 (1991) 3729.
123. Han, M., Lin, S.W., Smith, S.O. and Sakmar, T.P., J. Biol. Chem., 271 (1996) 32330.
124. Han, M., Lin, S.W., Minkova, M., Smith, S.O. and Sakmar, T.P., J. Biol. Chem., 271 (1996) 32337.
125. Strader, C.D., Fong, T.M., Tota, M.R. and Underwood, D., Annu. Rev. Biochem., 63 (1994) 101.
126. Choudhary, M.S., Sachs, N., Uluer, A., Glennon, R.A., Westkaemper, R.B. and Roth, B.L., Mol. Pharmacol., 47 (1995) 450.
127. Choudhary , M.S., Craigo, S. and Roth, B.L., Mol. Pharmacol., 43 (1993) 755.
128. Wess, J., Maggio, R., Palmer, J.R. and Vogel, Z., J. Biol. Chem., 267 (1992) 19313.
129. Fraser, C.M., Wang, C.-D., Robinson, D.A., Gocayne, J.D. and Venter, J.C., Mol. Pharmacol., 36 (1989) 841.
130. Savarese, T.M. and Fraser, C.M., Biochem. J., 283 (1992) 1.
131. Mansour, A., Meng, F., Meador-Woodruff, J.H., Taylor, L.P., Civelli, O. and Akil, H., Eur. J. Pharmacol., 227 (1992) 205.
132. Javitch, J.A., Li, X., Kaback, J. and Karlin, A., Proc. Natl. Acad. Sci. USA, 91 (1994) 10355.
133. Ho, B.Y., Karschin, A., Branchek, T., Davidson, N. and Lester, H.A., FEBS Lett., 312 (1992) 259.
134. Wang, C.-D., Gallaher, T.K. and Shih, J.C., Mol. Pharmacol., 43 (1993) 931.
135. Pollock, N.J., Mannelli, A.M., Hutchins, C.W., Steffey, M.E., MacKenzie, R.G. and Frail, D.E., J. Biol. Chem., 267 (1992) 17780.
136. Leurs, R., Smit, M.J., Tensen, C.P., Ter Laak, A.M. and Timmerman, H., Biochem. Biophys. Res. Commun., 201 (1994) 295.
137. Almaula, N., Ebersole, Zhang, D., Weinstein, H. and Sealfon, S., J. Biol. Chem., 271 (1996) 14672.
138. Blüml, K., Mutschler, E. and Wess, J., J. Biol. Chem., 269 (1994) 18870.
139. Javitch, J.A., Fu, D. and Chen, J., Biochemistry, 34 (1995) 16433.
140. Javitch, J.A., Fu, D., Chen, J. and Karlin, A., Neuron, 14 (1995) 825.
141. Strange, P.G., Trends Pharmacol. Sci., 17 (1996) 346.
142. Schwartz, T.W. and Rosenkilde, M.M., Trends Pharmacol. Sci., 17 (1996) 213.